

### 3. EXPLANATORY NOTES<sup>1</sup>

#### Shipboard Scientific Party<sup>2</sup>

#### INTRODUCTION

In this chapter, we have assembled information that will help the reader understand the basis for our preliminary conclusions and also help the interested investigator select samples for further analysis. This information concerns only shipboard operations and analyses described in the site reports in the *Initial Reports* volume of the Leg 160 *Proceedings of the Ocean Drilling Program*. Methods used by various investigators for shore-based analyses of Leg 160 data will be detailed in the individual scientific contributions published in the *Scientific Results* volume.

#### AUTHORSHIP OF SITE CHAPTERS

The separate sections of the site chapters were written by the following shipboard scientists (authors are listed in alphabetical order, no seniority is implied):

Principal Results: Emeis, Robertson  
Background and Objectives: Emeis, Robertson  
Geological Setting: Robertson  
Operations: Pollard, Richter  
Site Geophysics: Woodside  
Lithostratigraphy: Blanc-Valleron, Cramp, Flecker, Frankel, Kemp, Kopf, Major, Sakamoto  
Biostratigraphy and Sedimentation Rates: Di Stefano, Howell, Koizumi, Spezzaferri, Staerker  
Paleomagnetism: Roberts, Stoner  
Structural Geology: Flecker, Kopf  
Composite Depths: Janecek  
Inorganic Geochemistry: Brumsack, De Lange  
Organic Geochemistry: Bouloubassi, Rullkötter  
Physical Properties: Mart, Pribnow, Whiting  
Downhole Measurements: Jurado-Rodriguez, Rabaute, Woodside  
Heat-flow Measurements: Pribnow  
Summary and Conclusions: Emeis, Robertson  
Appendix: Shipboard Scientific Party

Following the text of the site chapter are summary core descriptions ("barrel sheets") and photographs of each core.

#### USE OF "Ma" VS. "m.y."

1. *Ma* is equivalent to and replaces *m.y.B.P.* (million years before present) to denote age, for example, 35–40 *Ma*.
2. *m.y.* is used to denote a number of years, such as ". . . for 5 *m.y.* in the early Miocene."

#### DRILLING CHARACTERISTICS

Information concerning sedimentary stratification in uncored or unrecovered intervals may be inferred from seismic data, wireline-logging results, and an examination of the behavior of the drill string, as observed and recorded on the drilling platform. Typically, the harder a layer, the slower and more difficult it is to penetrate. A number of other factors may determine the rate of penetration, so it is not always possible to relate the drilling time directly to the hardness of the layers. Bit weight and revolutions per minute, recorded on the drilling recorder, also influence the penetration rate.

#### Drilling Deformation

When cores are split, many show signs of significant sediment disturbance, including the concave-downward appearance of originally horizontal bands, haphazard mixing of lumps of different lithologies (mainly at the tops of cores), and the nearly fluid state of some sediments recovered from tens to hundreds of meters below the seafloor. Core deformation probably occurs during cutting, retrieval (with accompanying changes in pressure and temperature), and core handling on deck.

#### SHIPBOARD SCIENTIFIC PROCEDURES

##### Numbering of Sites, Holes, Cores, and Samples

Ocean Drilling Program (ODP) drill sites are numbered consecutively and refer to one or more holes drilled while the ship was positioned over one acoustic beacon. Multiple holes may be drilled at a single site by pulling the drill pipe above the seafloor (out of the hole), moving the ship some distance from the previous hole, and then drilling another hole.

For all ODP drill sites, a letter suffix distinguishes each hole drilled at the same site. The first hole drilled is assigned the site number modified by the suffix "A," the second hole takes the site number and suffix "B," and so forth. Note that this procedure differs slightly from that used by DSDP (Sites 1 through 624), but prevents ambiguity between site- and hole-number designations. It is important to distinguish among holes drilled at a site, because recovered sediments or rocks from different holes usually do not come from exactly equivalent positions in the stratigraphic column.

The cored interval is measured in meters below seafloor (mbsf). The depth interval assigned to an individual core begins with the depth below the seafloor that the coring operation began and extends to the depth that the coring operation ended (see Fig. 1). Each cored interval is generally 9.5 m long, which is the length of a core barrel. Coring intervals may be shorter and may not necessarily be adjacent if separated by drilled intervals. In soft sediments, the drill string can be "washed ahead" with the core barrel in place, without recovering sediments. This is achieved by pumping water down the pipe at high pressure to wash the sediment out of the way of the bit and up the space between the drill pipe and the wall of the hole. If thin, hard, rock layers are present, then it is possible to get "spotty" sampling of these resistant layers within the washed interval and thus to have a

<sup>1</sup>Emeis, K.-C., Robertson, A.H.F., Richter, C., et al., 1996. *Proc. ODP, Init. Repts.*, 160: College Station, TX (Ocean Drilling Program).

<sup>2</sup>Shipboard Scientific Party is given in the list preceding the Table of Contents.

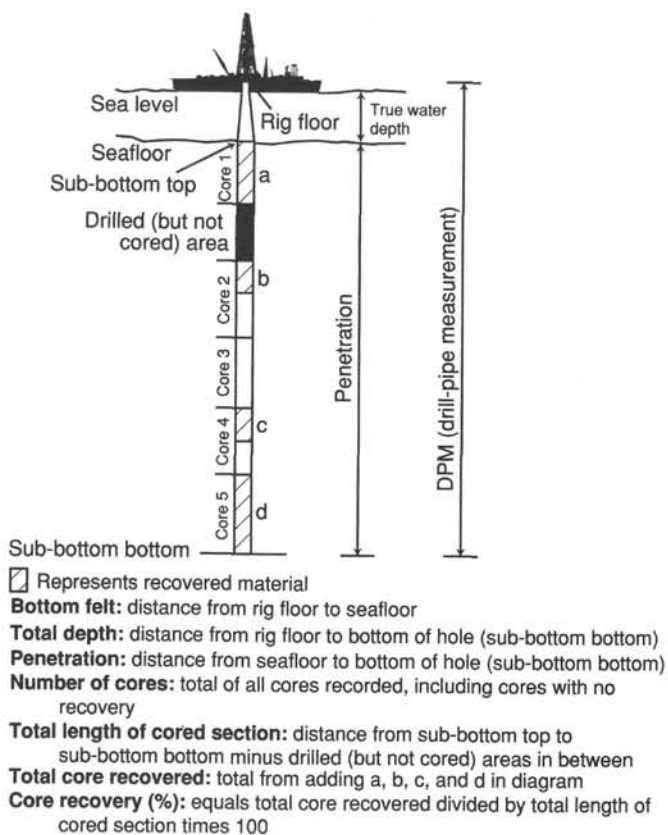


Figure 1. Coring and depth intervals.

cored interval greater than 9.5 m. When drilling hard rock, a center bit may replace the core barrel if it is necessary to drill without core recovery.

Cores taken from a hole are numbered serially from the top of the hole downward. Core numbers and their associated cored intervals in meters below seafloor ideally are unique in a given hole; however, this may not be true if an interval is cored twice, the borehole wall caves in, or other hole problems occur. Full recovery for a single core is 9.5 m of rock or sediment contained in a plastic liner (6.6-cm internal diameter) plus about 0.2 m (without a plastic liner) in the core catcher (Fig. 2). The core catcher is a device at the bottom of the core barrel that prevents the core from sliding out when the barrel is being retrieved from the hole. In many cores recovered with the extended core barrel or the advanced hydraulic piston corer, recovery exceeds the 9.5-m theoretical maximum by as much as 0.60 m. The cause of this expansion is not fully understood. The recovered core in its liner is divided into 1.5-m sections that are numbered serially from the top (Fig. 2). When full recovery is obtained, the sections are numbered from 1 through 7, with the last section generally being shorter than 1.5 m. Rarely, a core may require more than seven sections; this is usually the result of gas expansion having caused voids within some sections. When less than full recovery is obtained, as many sections as are needed to accommodate the length of the core will be used; for example, 4 m of core would be divided into two 1.5-m sections and a 1-m section. If cores are fragmented (recovery less than 100%), sections are numbered serially and intervening sections are noted as void, whether shipboard scientists believe that the fragments were contiguous in situ or not. In rare cases, a section less than 1.5 m may be cut to preserve features of interest. Some sections less than 1.5 m in length are also cut if the core liner is severely damaged.

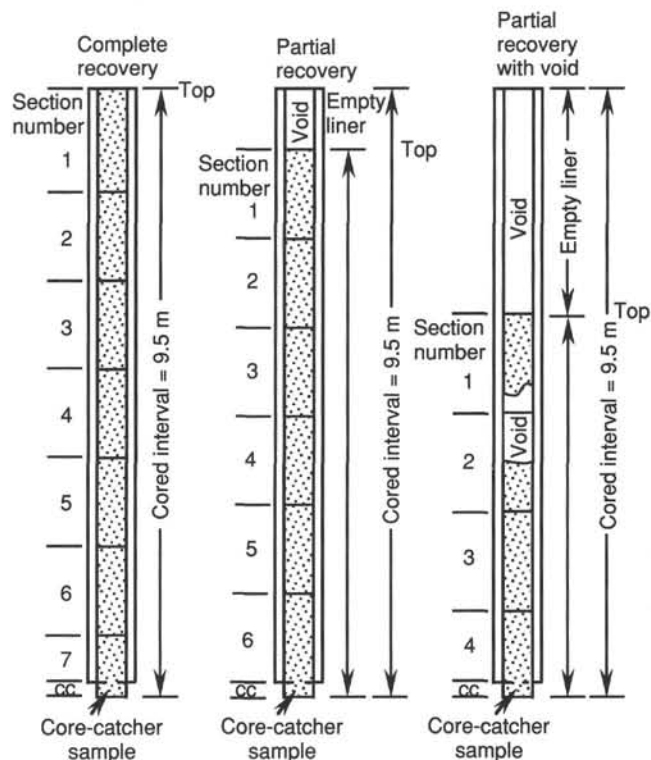


Figure 2. Examples of numbered core sections.

By convention, material recovered from the core catcher is placed immediately below the last section when the core is described and is labeled core catcher (CC); in sedimentary cores, it is treated as a separate section. The core catcher is assigned the depth of the top of the cored interval in cases where material is recovered only in the core catcher (this convention differs from that used in the early days of deep-sea drilling) although information from the driller of other sources may indicate from what depth it was actually recovered.

When the recovered core is shorter than the cored interval, the top of the core is equated with the top of the cored interval by convention, to achieve consistency when handling analytical data derived from the cores. Samples removed from the cores are designated by distance, measured in centimeters from the top of the section to the top and bottom of each sample removed from that section. A complete identification number for a sample consists of the following information: leg, site, hole, core number, core type, section number, piece number (for hard rock), and interval in centimeters, measured from the top of section. For example, a sample identification of "160-963A-15H-6, 10-12 cm" would be interpreted as representing a sample removed from the interval between 10 and 12 cm below the top of Section 6, Core 15 (H designates that this core was taken by the advanced hydraulic piston corer) of Hole 963A during Leg 160. A computer routine was available to calculate the depth in mbsf from any correctly formulated ODP sample designation; this avoids inconsistencies that frequently arise on those occasions where some sections were cut to nonstandard lengths. Although depth in mbsf is an invaluable convention, it is not ideal especially for high-resolution work; see the "Composite Depths" section (this chapter).

All ODP core and sample identifiers indicate core type. The following abbreviations are used: R = rotary core barrel (RCB); H = hydraulic piston core (HPC; also referred to as APC, or advanced hydraulic piston core); P = pressure core barrel; X = extended core barrel (XCB); B = drill-bit recovery; C = center-bit recovery; I = in

situ water sample; S = sidewall sample; W = wash-core recovery; and M = miscellaneous material. APC, XCB, RCB, and W cores were cut during Leg 160.

### Core Handling

As soon as a core was retrieved on deck, a sample taken from the core catcher was given to the paleontological laboratory for an initial age assessment. Special care was taken in transferring the core from the drill floor to a long horizontal rack on a catwalk near the core laboratory so that the core did not bend or twist excessively. The core was capped immediately, and gas samples were taken by piercing the core liner and withdrawing gas into a vacuum tube. Voids within the core were sought as sites for gas sampling. Some of the gas samples were stored for shore-based study, but others were analyzed immediately as part of the shipboard safety and pollution-prevention program. Next, the core was marked into section lengths of 150 cm, each section was labeled, and the core was cut into sections. Interstitial water (IW) and whole-round physical properties (PP) samples were also taken at this time. In addition, some headspace gas samples were taken from the end of cut sections on the catwalk and sealed in glass vials for light hydrocarbon analysis. Afterward, each section was sealed at the top and bottom by gluing on color-coded plastic caps: blue to identify the top of a section and clear for its bottom. A yellow cap was placed on the section ends from which a whole-round sample had been removed. The caps were usually attached to the liner by coating the end liner and the inside rim of the cap with acetone and then attaching the caps to the liners.

The cores were then carried into the laboratory, where the sections were labeled with an engraver to mark the complete designation of the section permanently. The length of the core in each section and the core-catcher sample were measured to the nearest centimeter. This information was logged into the shipboard CORELOG database program.

Whole-round sections from APC and XCB cores normally were run through the multisensor track (MST). The MST includes the gamma-ray attenuation porosity evaluator (GRAPE), *P*-wave logger, natural gamma-ray emission measurement device, and volume magnetic susceptibility meter. The core-catcher sample is not run through the MST track, for which reason we avoided using it for final biostratigraphic work. In most cases, the temperature of each core was measured prior to MST analysis. After the core had equilibrated to room temperature (approximately 3 hr), soft sediments were measured for thermal conductivity prior to being split. Cores were split lengthwise into working and archive halves. Softer cores were split with a wire. Harder cores were split using a diamond saw. The wire-cut cores were split from the top to bottom so that sediment below the voids or soupy intervals that may be present at the top of Section 1 would not be drawn into the voids.

After splitting, working and archive halves of each section were designated. The archive half then was described visually. Smear slides were made from samples taken from the archive half and the reflective characteristics were measured with a hand-held spectrophotometer. This was followed by our running the archive half of the core through the cryogenic magnetometer. Finally, the cores were photographed with both black-and-white and color film, a whole core at a time. Close-up photographs (black-and-white) were taken of particular features, as requested by individual scientists, for illustrations in the summary of each site. The archive halves of cores from the second complete hole at each site (generally the "C" hole) were run through the cryogenic magnetometer prior to description to provide those scientists sampling physical properties guidance in choosing sample intervals so as not to disturb significant magnetic reversal boundaries. The archive halves were then described visually and finally photographed.

The working half of the core was measured first for sonic velocity and vane shear strength. After physical properties sampling, the working half was sampled for reconnaissance-level and low-resolution shipboard and shore-based laboratory studies. Most of the sampling for detailed high-resolution paleoceanographic and paleoclimatic studies was deferred until after the cruise to optimize the sampling with the stratigraphic information from the biostratigraphy, paleomagnetic stratigraphy, and lithologic correlations.

Each sample taken either for shipboard or shore-based analysis was logged into the sampling database program by the location and the name of the investigator receiving the sample. Records of all of the samples removed are kept by the curator at ODP headquarters. The extracted samples were sealed in plastic vials or bags and labeled. Samples were routinely taken for shipboard physical property and geochemical analyses. These data are reported in the site chapters.

Both halves of the core were placed into labeled plastic tubes, which were then sealed and transferred to cold-storage space aboard the drilling vessel. At the end of the leg, the cores were transferred from the ship in refrigerated air-freight containers to cold storage in the Bremen Repository of the Ocean Drilling Program, University of Bremen, Germany.

## LITHOSTRATIGRAPHY

### Core Description

The following section summarizes established ODP conventions used for compiling core description forms (cf., Mazzullo et al., 1987) and the revisions made to these procedures as adopted during Leg 160.

Leg 160 sedimentologists were responsible for visual core logging, smear-slide analyses, thin-section descriptions, and high-resolution sediment color analysis. This information, together with the biostratigraphic data, was used to compile a Visual Core Description (VCD) form for each core (for example, Core 160-966A-1H, see Fig. 3). The VCD forms are presented together with magnetic susceptibility, GRAPE, and color reflectance data, and core photographs in Section 5 of this volume and on the CD-ROM (back pocket).

### Core Identification

Cores are identified using leg, site, hole, core number, and core type (see "Introduction" section, this chapter). The depth of the cored interval is specified in terms of meters below seafloor. When necessary for interhole and/or intersite comparison, lithostratigraphic data are presented with reference to meters composite depth (mcd; see "Composite Depths" section, this chapter).

### Graphic Lithology Column

The lithology of the recovered material is represented on the core description form by up to three symbols in the column titled "Graphic Lithology" (Figs. 3, 4). Where an interval of sediment or sedimentary rock is a homogeneous mixture, the constituent components are separated by a solid vertical line, with each component represented by its own symbol. Components accounting for <10% of the sediment in a given lithology are not shown in the "Graphic Lithology" column. In an interval comprising two or more sediment lithologies that have different compositions and are thinly interbedded, the average relative abundances of the lithologic constituents are represented graphically by dashed lines that vertically divide the interval into appropriate fractions, as described above. Because of the limited scale of the core summaries, the "Graphic Lithology" column shows only the composition of layers exceeding approximately 16 cm in



thickness. These may be indicated by the banding symbol in the "Structure" column and in the lithologic description text on the VCD form.

### Chronostratigraphy

The chronostratigraphic unit, as recognized on the basis of paleontological criteria, is shown in the "Age" column. The biostratigraphic zonations used are presented in the "Biostratigraphy" section of this chapter.

### Sedimentary Structures

In sediment cores, natural structures and structures created by the coring process can be difficult to distinguish. Natural sedimentary structures observed are indicated in the "Structure" column of the core description form. The column is divided into three vertical areas. The intensity of bioturbation is shown in the central portion of the "Structure" column of the VCD in the conventional manner (slight, moderate, heavy). The symbols on the two side portions of the "Structure" column indicate the location of individual bedding features, thin color banding, and any other sedimentary features, such as nodules, disseminated pyrite, and discrete trace fossils such as *Zoophycos*. An example of the layout of the "Structure" column from the VCD form is provided in Figure 5. The symbols used to describe each of these primary and secondary biogenic and physical sedimentary structures are presented in Figure 6.

### Sedimentary Disturbance

Sediment disturbance resulting from the coring process is shown in the "Disturbance" column of the core description form. Blank regions indicate an absence of drilling disturbance. The degree of drilling disturbance is described for soft and firm sediments using the following categories:

1. Slightly disturbed: bedding contacts are slightly deformed;
2. Moderately disturbed: bedding contacts have undergone extreme bowing;
3. Highly disturbed: bedding is completely deformed as flow-in, coring/drilling slough, and other soft-sediment stretching and/or compressional shearing structures attributed to the coring/drilling process; and

4. Soupy: intervals are water saturated and have lost all traces of original bedding.

The degree of fracturing in indurated/lithified sediments is described using the following categories:

1. Slightly fractured: core pieces are in place and broken;
2. Moderately fractured: core pieces are in place or partly displaced, and the original orientation is preserved or recognizable (drilling slurry may surround fragments, i.e., drilling/coring "biscuits" are evident);
3. Highly fractured: core pieces are from the interval cored and probably in the correct stratigraphic sequence (although they may not represent the entire section), but the original orientation is completely lost; and

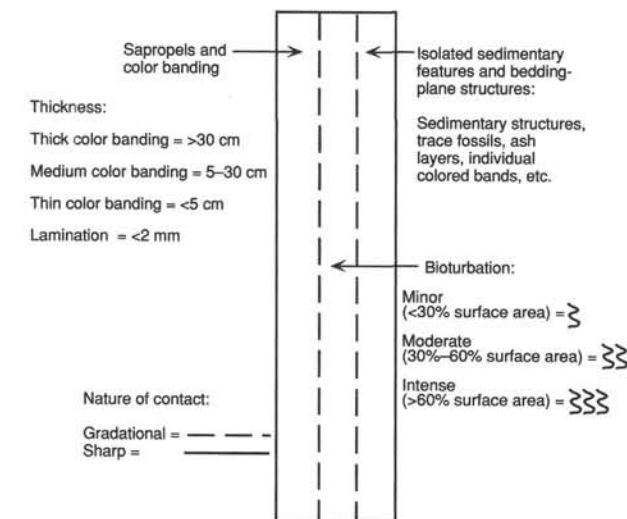


Figure 5. Layout of the sedimentary "Structure" column on the VCD form shown in Figure 3.

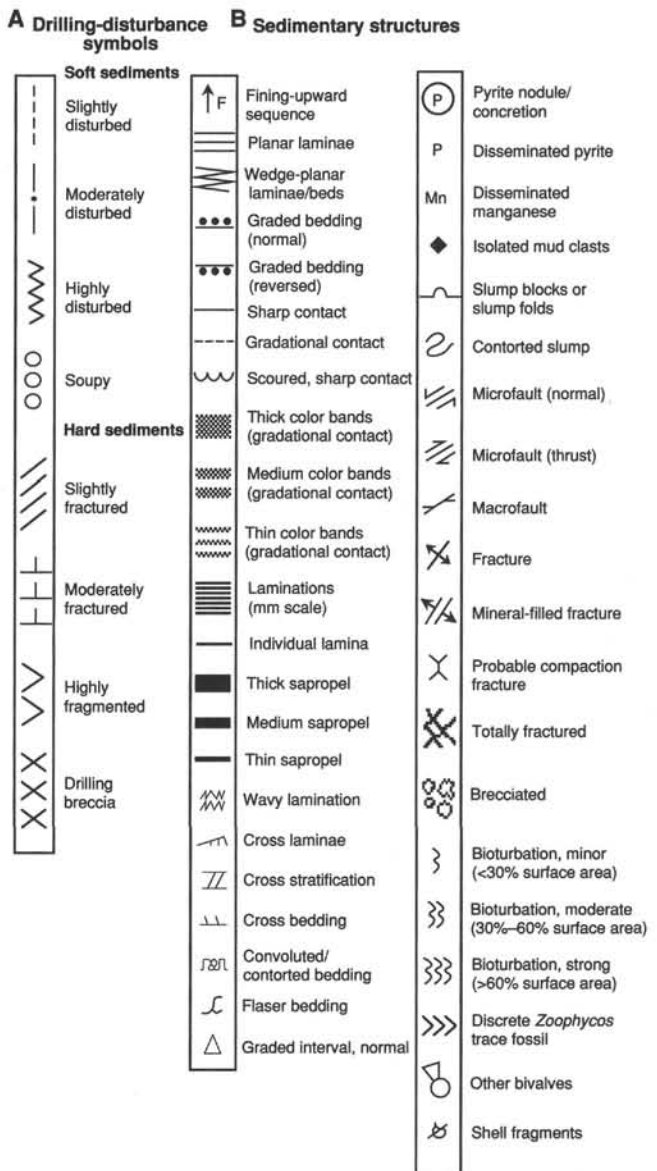


Figure 6. A. Symbols used for drilling disturbance in the "Disturbance" column of the visual core description form. B. Symbols used to indicate color banding, bioturbation, and isolated sedimentary structures/trace fossils/macrossediments in the "Structure" column of the VCD form.

4. Drilling breccia: core pieces have lost their original orientation and stratigraphic position and may be mixed with drilling slurry.

### Color

The hue and chroma attributes of color (Munsell) were determined using the hand-held Minolta CM-2002 spectrophotometer as soon as possible after the cores were split. The color scanner was also used to measure reflected visible light in the range between 400 and 700 nm. These reflectance measurements were routinely taken at 2- to 5-cm intervals on all cores and were augmented with additional readings across distinct lithologic boundaries.

### Samples

The position of samples taken from each core for shipboard analysis is indicated in the "Sample" column on the core description form. The symbol "S" indicates the location of smear-slide samples, the symbol "T" indicates the location of thin-section samples, and the symbol "M" indicates the location of paleontology samples. The notations "T" and "P" designate the location of samples for whole-round interstitial water geochemistry and physical property analyses, respectively.

### Smear-slide Summary

A table summarizing data from smear-slide and thin-section analyses appears in Section 6 of this *Initial Reports* volume. This table includes information about the sample location, whether the sample represents a dominant (D) or a minor (M) lithology in the core, and the estimated percentages of sand, silt, and clay, together with all identified components.

### Lithologic Description

The lithologic description that appears on each VCD consists of three components:

1. A heading that lists the major sediment lithologies observed in the core;
2. A general description of these sediments, including location, occurrence, and frequency of significant features such as color banding; and
3. The description and location of minor lithologies such as individual beds/layers and trace fossils.

Reference is also made in the description to sediment disturbance produced by natural processes and/or by the coring/drilling process. A description of structural features is given in the "Structural Geology" section (this chapter).

### Classification

Leg 160 sedimentologists adopted the standard ODP sediment classification of Mazzullo et al. (1987). The classification identifies a granular sediment by designating a principal name (sediment class) together with major and minor modifiers (texture, composition, and fabric) (Fig. 7).

#### Principal Names

For *pelagic* sediment, the principal name describes the composition and degree of consolidation using the following terms:

1. Ooze: unconsolidated calcareous and/or siliceous biogenic sediments;

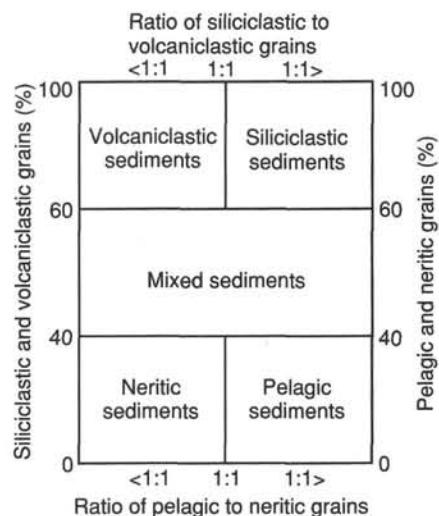


Figure 7. Sediment classification scheme adopted for Leg 160.

2. Chalk: firm biogenic sediment composed predominantly of calcareous biogenic grains with shear strengths >200 kPa; and
3. Limestone: hard pelagic sediment composed predominantly of calcareous pelagic grains.

For *siliciclastic* sediment, the principal name describes the texture and is assigned according to the following guidelines:

1. The Udden-Wentworth grain-size scale (Wentworth, 1922) defines the grain-size ranges and the names of the textural groups (gravel, sand, silt, and clay) and subgroups (fine sand, coarse silt, etc.) that are used as the principal names of siliciclastic sediment;
2. If two or more textural groups or subgroups are present in a siliciclastic sediment, they are listed as principal names in order of increasing abundance; and
3. The suffix "-stone" is affixed to the principal names sand, silt, and clay if the sediment is lithified.

#### Major and Minor Modifiers

The principal name of a granular sediment class is preceded by major modifiers and is followed by minor modifiers (preceded by the term "with") that describe the lithology of the granular sediment in greater detail. The most common use of major and minor modifiers is to describe the composition and textures of grain types that are present in major (>25%) and minor (10% to 25%) proportions. Note that modifiers are always listed in order of increasing abundance. For example, an unconsolidated pelagic sediment containing 30% clay, 15% foraminifers, and 55% nannofossils would be called a clayey nannofossil ooze with foraminifers.

#### Sapropel Nomenclature and Sapropel Description Sheets

Leg 160 decided not to adopt the much cited nomenclature proposed by Kidd et al. (1978) because this quantitative definition produces an arbitrary division between organic-rich sediments based on organic carbon content, which may not accurately reflect the depositional process. The definition proposed by Hilgen (1991b) was adopted to describe all organic-rich sediments recovered. As such, the term "sapropel" is used to define *all* organic-rich sediments.

As one of the main objectives of Leg 160 was to investigate the depositional history of organic-rich sediment (sapropel) layers in the Mediterranean, a standardized sapropel description sheet was pro-





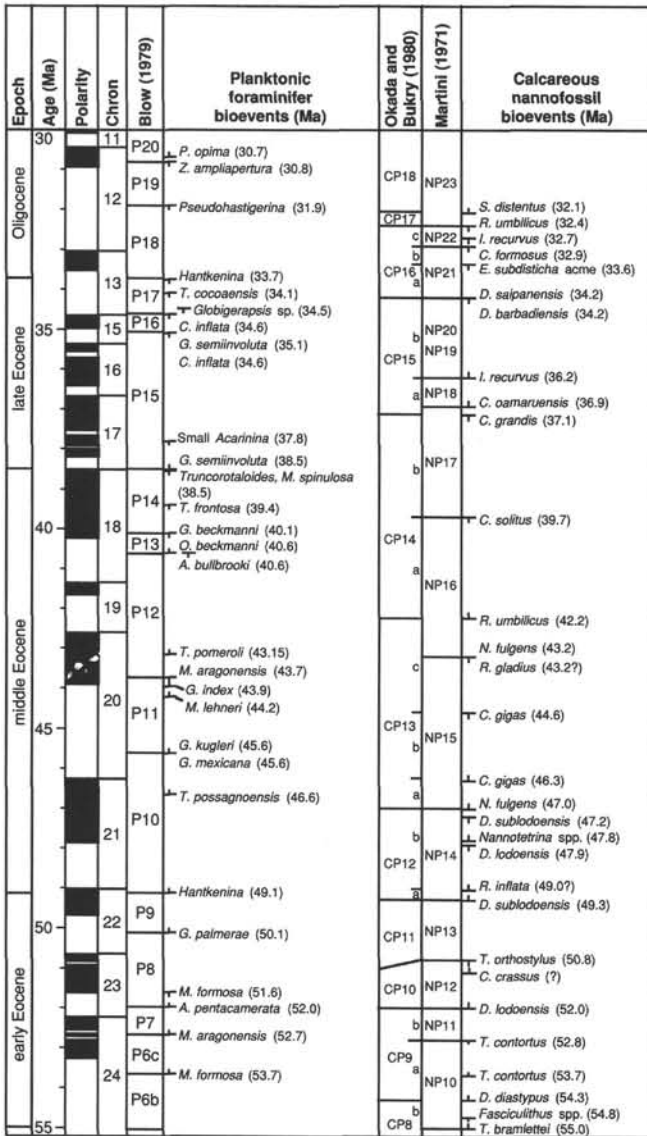


Figure 11. Correlation of Eocene to Oligocene nannofossil and foraminiferal events with the geomagnetic polarity time scale of Cande and Kent (1992). From Larsen, Saunders, Clift, et al. (1994), modified after I. Premoli Silva and S. Monechi (pers. comm., 1994).

P = poor: severe fragmentation, heavy overgrowth, and/or dissolution.

Typical planktonic foraminiferal assemblages for each slide were recorded in the micropaleontological program FossilList.

**Bolboforma**

Bolboforma is a protophyte *incertae sedis*, probably a calcareous algae, typical of high to middle latitudes. Bolboforma is an important marker for Eocene, lower Oligocene, and middle Miocene to lower Pliocene sediments, especially where all other calcareous microfossils are absent or removed by dissolution. In the Mediterranean Sea this microfossil is poorly known; however, its presence is documented in several DSDP holes and outcrops in the central Paratethys (Spiegler and Rögl, 1992).

The samples analyzed for planktonic foraminiferal content are also suitable for Bolboforma studies.

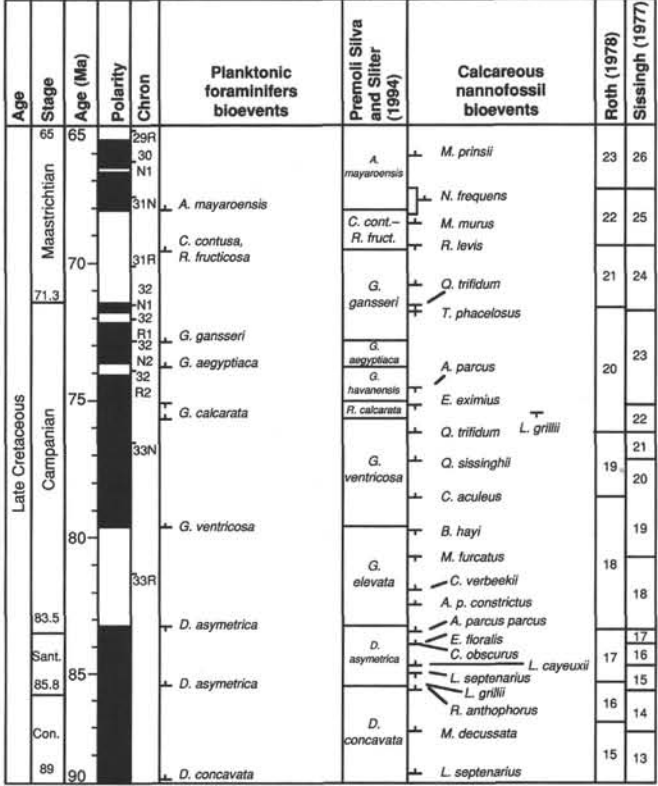


Figure 12. Correlation of Late Cretaceous nannofossil and foraminiferal events with the geomagnetic polarity time scale of Gradstein et al. (1994). From Erba et al. (in press).

Table 1. Dates of Pliocene-Pleistocene magnetic polarity boundaries (after Cande and Kent, 1995).

Normal polarity interval (Ma)	Polarity chron
0.000–0.780	C1n
0.990–1.070	C1r.1n
1.770–1.950	C2n
2.140–2.150	C2r.1n
2.581–3.040	C2An.1n
3.110–3.220	C2An.2n
3.330–3.580	C2An.3n
4.180–4.290	C3n.1n
4.480–4.620	C3n.2n
4.800–4.890	C3n.3n
4.980–5.230	C3n.4n

**Paleoenvironmental Interpretation**

In addition to biostratigraphic applications, microfossils were used for paleoenvironmental interpretation. Where applicable, relative paleodepth evaluations were made using both planktonic and benthic foraminifers. Presence, abundance, and species diversity of all microfossils identified during Leg 160 will also allow paleoclimatic interpretation of the Mediterranean Sea through time.

**PALEOMAGNETISM**

**Laboratory Facilities**

The shipboard paleomagnetic laboratory is equipped with two magnetometers: a pass-through cryogenic superconducting rock magnetometer manufactured by 2-G Enterprises (model 760R) and a

Molspin spinner magnetometer. The sensing coils in the cryogenic magnetometer measure the magnetization over an interval of approximately 15 cm, with the coils for each axis having slightly different response curves. The large volume of material sensed (about 200 to 300 cm<sup>3</sup>) gives the cryogenic system excellent sensitivity despite the relatively high background noise aboard the ship. An alternating field (AF) demagnetizer, capable of peak AFs of 35 mT (2-G model 2G600) is aligned with the pass-through system. Peak AFs of 20–25 mT were used routinely during Leg 160 because constant use at higher field settings can cause excessive heating of the demagnetizing coils.

The magnetic susceptibility of unsplit core sections was measured using a Bartington Instruments model MS1 susceptibility meter attached to a MS1/CX 80-mm whole-core sensor loop that operates at 0.465 kHz. The full width of the impulse response peak (at one-half maximum) is less than 5 cm. The susceptibility loop is mounted in line with the other physical properties sensors (GRAPE, natural gamma, and *P*-wave) on the multisensor track.

Stepwise demagnetization of single samples was normally achieved with a Schonstedt model GSD-1 AF demagnetizer, which is capable of demagnetizing discrete samples to 100 mT. Thermal demagnetization was not conducted owing to the time constraints imposed by the high rate of core recovery during Leg 160.

Ancillary laboratory equipment available during Leg 160 included a Kappabridge KLY-2 susceptibility bridge, which was used for most discrete sample measurements of bulk susceptibility and for determining the anisotropy of magnetic susceptibility. A DTECH magnetizer was used to impart anhysteretic remanent magnetizations with a peak AF of 100 mT and a bias field of 0.05 mT, and an ASC impulse magnetizer was used to produce isothermal remanent magnetizations.

### Paleomagnetic Measurements

Virtually all of the paleomagnetic measurements were made using the cryogenic magnetometer. The bulk of these were made on archive-half sections. Pass-through paleomagnetic measurements were made on the archive halves of the 1.5-m core sections for all APC cores for every hole at each site. We routinely measured the natural remanent magnetization (NRM) after AF demagnetization at either 20 or 25 mT at 10-cm measurement intervals. Because of the limitations of the long-core measurement technique, difficulties were encountered in obtaining reliable paleomagnetic results from the sediments recovered during Leg 160 (see Roberts et al., this volume, for a more complete description). It was therefore necessary to undertake full stepwise demagnetization of discrete samples to elucidate the magnetic polarity stratigraphy at most sites.

The ODP core orientation convention designates the X-axis as the horizontal (in situ) axis radiating from the center of the core through the space between a double line inscribed lengthwise on the working half of each core liner. All declinations reported are relative declinations measured with respect to this double line.

### Core Orientation

Orientation of the APC cores was conducted using the Tensor orientation tool. This tool consists of a three-component fluxgate magnetometer and a three-component accelerometer that are rigidly attached to the core barrel and record the drift of the hole and orientation of the double fiducial line on the plastic core liner. The Tensor tool was set to record at 30-s intervals. The data were downloaded from the tool after several APC runs. All of the internal memory of the tool (1023 shots) was written to a file, which was named to describe the hole as well as the first and last cores recorded in the file (e.g., file "963B1924" contains data from Tensor tool shots taken for Cores 160-963B-19H through 24H). Core orientation was not attempted for the first two APC cores at each site, before the mud line was established. This precluded the possibility of damage to the ori-

entation tool owing to the shock of a corer stroking out above the mud line. Otherwise, core orientations were taken for most APC cores. Notes on orientation tool runs (start time, hold-off time, tool number, and bottom time) were included in a file titled "SHOTS.TXT."

In cases where no orientation data were available from the Tensor tool, the measured declinations from the discrete-sample measurements, averaged to 0° for normal polarity and averaged to 180° for reversed polarity, were used to orient the core. Where sufficient data were available, these orientations were supplied to the structural geologists to assist in structural analyses of core material.

### Low-field Susceptibility

Whole-core volume magnetic susceptibility was measured using the automated MST in conjunction with the GRAPE, natural gamma, and *P*-wave sensors. The magnetic susceptibilities were sufficiently strong to enable measurement on whole-round sections with the Bartington MS1 magnetic susceptibility meter using the low-sensitivity (1.0) range. All measurements were taken in the cgs mode. Susceptibility data were archived in raw instrument units, which require a single multiplicative factor of  $7.7 \times 10^{-6}$  to convert to volume-normalized SI units. This calibration factor was checked by comparing MST susceptibility values over several selected intervals against measurements of discrete samples done with the Kappabridge susceptibility meter.

### Magnetostratigraphy

Where demagnetization successfully isolated the primary component of remanence, paleomagnetic inclinations were used to assign a magnetic polarity to the stratigraphic column. Interpretations of the magnetic polarity stratigraphy, with constraints from the biostratigraphic data, are presented in the site chapters. During Leg 160, the chron nomenclature from the magnetic polarity time scale of Cande and Kent (1992) was used. However, Cande and Kent (1995) have modified their time scale to incorporate the astronomically calibrated ages of the Pliocene-Pleistocene polarity boundaries given by Hilgen (1991a, 1991b) and Shackleton et al. (1990). The time scale of Cande and Kent (1995) has therefore been adopted for all polarity boundaries identified in the sediments recovered during Leg 160.

## STRUCTURAL GEOLOGY

The purpose of structural core descriptions is to systematically and quantitatively identify and describe structural features (including bedding) present in the core. Apart from the whole-round samples taken immediately after core recovery, material from both the working and archive halves was examined. The responsibilities of shipboard structural geologists include

1. Documenting all structures in the core and information concerning the relative timing of the various structures and diagenetic events.
2. Recording the orientation of all structures on the core face and wherever possible, orienting these in three dimensions in the core reference frame.
3. Reorienting structural features from the core reference frame into a geographic framework by applying Tensor orientation tool data and Formation MicroScanner (FMS) data. It was not possible to use primary remnant magnetization orientations to reorient structural information because of the complicated nature of the paleomagnetic signal measured (see "Paleomagnetism" section, this chapter).
4. Obtaining evidence from the style, geometry, and microstructure of individual structures that may have a bearing on the processes and conditions of deformation and on finite strain.

5. Constructing plausible interpretations of tectonic environments and deformation history within the limitations of the shipboard data set.

### Limitations

Several problems are inherent in this type of study: incomplete core recovery, drilling-induced deformation, and rotation. Incomplete core recovery may lead to a sampling bias that is particularly acute for structural purposes. For example, material from fault zones is typically not recovered. When faulted rock is recovered, original deformation patterns may be disturbed. It can be difficult to distinguish between drilling-induced disturbance and real tectonic features. Planar structures that traverse a core and are associated with preserved fault rock may be regarded as original tectonic features rather than drilling-induced artifacts. In soft sediments, the degree of disruption of the bedding and other sedimentary structures and the orientation of the structures relative to the side of the core liner can be used as an indication of core-induced ductile disturbance. However, the identification of drilling-related brittle features in layered sediments where the lithologic contrast from layer to layer is high has proved problematic. It is hoped that post-cruise statistical analysis of large fault populations and experimental work will help resolve this issue. Cemented and/or mineral-lined fractures are geological phenomena. Gently plunging striations or polishing marks may be drilling induced, but these can usually be distinguished from preexisting slickensides owing to their orientation. Features should be considered drilling induced if their origin is in doubt.

Features are initially oriented relative to local reference coordinates (i.e., the core liner reference frame) and subsequently corrected to geographic north and vertical. Potentially, this can be done with data from the Tensor orientation tool (with the APC system only), paleomagnetic study, and the FMS.

### Formation MicroScanner

The FMS downhole logging tool is described in the "Downhole Measurements" section of this chapter. FMS logging can be used most successfully for orientation purposes where, for example, regularly inclined bedding or a single, regular joint pattern can be recognized on downhole images and correlated with the core-derived data (e.g., MacLeod et al., 1992, 1994). These images are oriented with respect to geographical coordinates using built-in triaxial magnetometers. Comparison of the features in the cores and on the logs therefore allows the former to be reoriented from the core reference frame to geographical coordinates. Low recovery and the absence of distinctive markers in the borehole may inhibit correlation and reorientation. Detailed comparison of the FMS data with the logs can be made only post-cruise.

The FMS tool was used only in the longer holes at the tectonic sites (e.g., Eratosthenes Seamount and the mud volcano sites).

### Tensor Orientation Tool

The Tensor orientation tool provides frequent measurements of the direction and degree of deviation of the hole from the vertical (see "Downhole Measurements" section, this chapter). This tool allows orientation of the APC cores with respect to magnetic north and, hence, positions the arbitrary core reference frame. For XCB and RCB coring, however, rotation of individual rock pieces within the core barrel is common and prohibits use of the Tensor orientation tool. Because of the nature of the top of holes it was generally not possible to use the Tensor tool until Core 3. After obtaining measurements only for one or two of the four to six holes drilled at each of the first two sites, the Tensor tool was run in all APC holes greater than three cores deep.

## Core Descriptions

The shipboard structural geologist makes a sketch of the core on the Structural Core Description form (Fig. 13). Features such as bedding, folds, and faults are assigned a sequential reference number. If a core length is relatively devoid of features, the structural geologist may opt not to draw this interval, but merely mark features on the data table (Fig. 14). The feature number is used to link data in the data table to drawings of the feature on the VCD form. In the data table (Fig. 14), the feature is identified using the codes defined in the accompanying list of structural terms (Table 2). The core drawings are scanned and stored as Macintosh PICT files and are found on the CD-ROM in the back pocket of this volume. The working terminology for macroscopic features is shown in Table 2. Gradation and overlap between different features are identified by adding modifiers, descriptive comments, and sketches. Symbols for structures entered in the barrel sheets (see "Lithostratigraphy" section, this chapter) are listed in Figure 6.

Fractures and faults are distinguished from each other on the basis of reasonable evidence for displacement, including truncation or offset of passive markers and the presence of slickensides and striations, fault gouge, or breccia. Veins are characterized by their fill, width, and presence or absence of an alteration halo. The orientation of structural features is noted relative to the core coordinates (Fig. 15).

### Measurement of Structures

The orientation of structures is measured using a protractor-like graduated scale, with a pivoting, transparent measuring arm. During measurement, one-half of the arm is aligned with the structure and the other half points to the value of the dip angle on the graduated scale. The apparent dip of features can be determined, both parallel to the split core face and at right angles to it (i.e., along surfaces where the core has broken or material has been artificially removed; cf., Fig. 15). The measurement of two different apparent dips on a structure allows calculation of the "true" dip and dip direction. The RUNFORT computer program can be used to generate the true dip and dip direction by calculating the cross product of two apparent dips. During Leg 160, wherever multiple holes were drilled at a single site and sapropels recovered, the sampling policy excluded the measurement of structural features in anything other than the plane of the core face in at least two of the holes. For these holes, although apparent dip measurements in the core face plane were recorded on the table and the features drawn on the VCD forms, it was not possible to calculate the true dip and dip direction. Similarly, in order to keep the sapropels as intact as possible both for shipboard and post-cruise sampling, cutting the core within the sapropels to measure a second apparent dip on bedding surfaces or fault planes was heavily discouraged. In many cases, it was possible to measure the orientation of a geochemical front above or below a sapropel as a proxy for bedding orientation, although because of sampling restrictions it was not possible to ascertain the error of the inherent assumption that the geochemical front is parallel to the bedding. Sharp color changes were therefore used only where they could be seen to be parallel on the core face to lithologic boundaries that could not be measured in three dimensions, as noted in the "Comments" column of the data table.

The plane normal to the axis of the borehole is referred to as the apparent horizontal plane. On this plane, a 360° net is used with a "pseudo-north" (000°) at the bottom line of the working half of the core. The face of the split core, therefore, lies in a plane striking 90°–270° and dips vertically (see Fig. 15).

### Thin-section Descriptions

Thin sections were examined (1) to confirm macroscopic descriptions of ductile and brittle structures, (2) to provide kinematic infor-

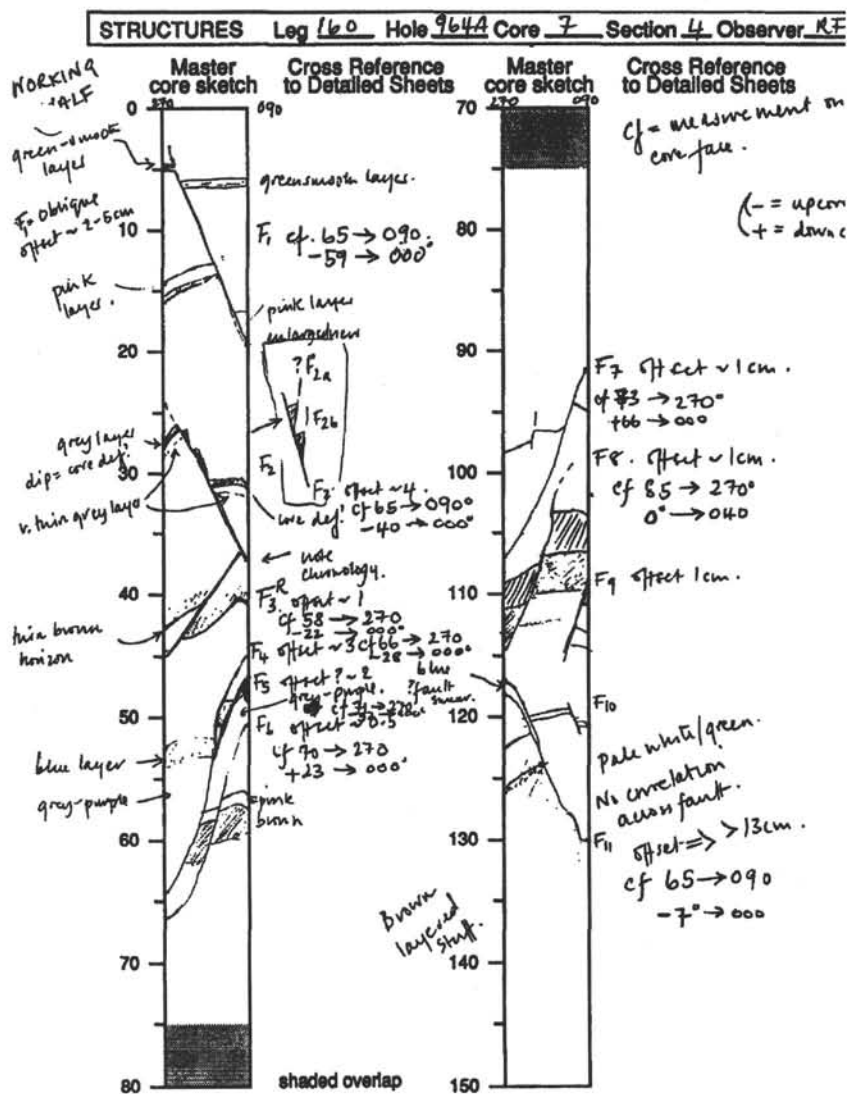


Figure 13. Structural Core Description form. The vertical scale is in centimeters below the top of the cored interval.

mation, (3) to determine time relationships between different deformational features, and (4) to provide coverage of both major structural zones and representative downhole variations.

Sections of rock or indurated sediment were generally oriented with respect to the core coordinates and cut parallel to the core axis (and the direction of plate convergence at the tectonic sites). However, at the mud volcano sites, lithified clasts within the matrix are apparently randomly oriented and these clasts were therefore cut in the direction though most suitable for displaying the structure within them. The information obtained from microscopic studies of thin sections was entered on the standardized structural forms and into the SLIDES database and is on the CD-ROM in the back pocket of this volume.

## COMPOSITE DEPTHS

### Composite Section Development

The recovery of continuous sections over APC-cored intervals of the sedimentary sequence was crucial to the paleoceanographic objectives of Leg 160. Drilling multiple APC holes offset in depth at each site has traditionally helped to ensure that intervals of no recovery in a single APC hole were recovered in an adjacent hole. During Leg 160, as with previous ODP legs, the continuity of recovery was

confirmed by the development of composite depth sections at the multiple-cored sites. The methodology used for composite section development during Leg 160 is similar to that used to construct composite depth sections during Leg 154 (Curry, Shackelton, Richter, et al., in press) and is briefly summarized below.

At each site, high-resolution (2- to 10-cm interval) measurements of magnetic susceptibility, GRAPE wet-bulk density, natural gamma, and P-wave velocity were made on the multisensor track soon after the cores were retrieved. Additionally, measurements of visible percent color reflectance were made at 2-cm resolution on the split cores (see "Lithostratigraphy" section, this chapter). Using color reflectance and magnetic susceptibility as the primary lithologic parameters, the measurements from each hole were visually and quantitatively compared to determine if coring offsets were maintained between holes. The correlation of events present in multiple holes provided verification of the extent of recovery of the sedimentary sequence. Integration of at least two different physical properties allowed hole-to-hole correlations to be made with greater confidence than would be possible with only a single parameter.

Hole-to-hole correlations were made using interactive software developed specifically for this task. We used a prototype software package that was developed at Lamont-Doherty Earth Observatory and patterned after the Leg 138 core-correlation software (Hagelberg et al., 1992). Corresponding features in the data from cores in adja-

Leg : 160 Site : 964 Hole : A Observers : RF / KOP

Core	Section	Depth (cm)		Pitce #	Depth (mbsf)	Feature #	Offset Width (cm)	Orientation on core face		2nd appt. orientation		Calculated Orientation		Geographic Orientation		Comments
		top	base					appt. dip	direction	appt. dip	direction	dip	direction	dip	direction	
7H	4	4	19			F <sub>1</sub>	3	65	090	59	180					Normal
7H	4	24	37			F <sub>2</sub>	4	65	090	40	180					Normal
7H	4	36	45			F <sub>3</sub>	1	56	270	22	180					Reverse
7H	4	45	64			F <sub>4</sub>	3	66	270	28	180					Lithic normal ft. with slip
7H	4	47	53			F <sub>5</sub>	2	71	270	52	180					Normal
7H	4	50	67			F <sub>6</sub>	0.5	70	270	23	000					Normal
7H	4	92	107			F <sub>7</sub>	1	73	270	66	000					Normal
7H	4	100	114			F <sub>8</sub>	1	85	270	0	040					Normal
7H	4	110	115			F <sub>9</sub>	1									Normal
7H	4	119	122			F <sub>10</sub>	0.5									Normal
7H	4	118	130			F <sub>11</sub>	>13	65	090	7	180					Normal

Figure 14. Structural data form used for collecting measured structural information and reoriented structural directions where possible. The feature number is used for cross reference to the Structural Core Description form.

Table 2. List of structural features identified in cores and their abbreviations for use on the structural data table and VCD form.

Structural feature	Identifier abbreviation	Planar or linear orientation measured
Drilling induced	DI	
Joint	J	Joint surface
Mineral vein	V	Vein margin
Fault	F	Fault plane
Slickenside	SL	Slickenside plunge and plunge direction
Fold	Fo	Fold plane and hinge line
Slump fold	SFo	Fold plane and hinge line
Shear zone	SZ	Shear zone margin
Gradational boundary	GB	Approximate planar boundary orientation
Sedimentary bedding	SB	Bedding plane
Color change	SB/C	Planar color change
Slump	SP	Slump bounding surfaces
Fracture	FR	Fracture plane
Discontinuity	DIS	Discontinuity plane
Dominant fabric	DF	Fabric plane

Note: Numerical subscripts to the abbreviations refer to scanned sketches on the VCD forms on the CD-ROM (back pocket).

cent holes were aligned using both graphical and quantitative cross-correlations. Correlative features were aligned by adjusting the ODP depths in meters below seafloor for a given core, on a core-by-core basis. No depths were adjusted within a given core. The results from the multiple lithologic parameters (primarily magnetic susceptibility and color reflectance) were integrated to resolve discrepancies. The resulting adjusted depth scale is in meters composite depth (mcd). For each core at each site, the depth adjustment required to convert from mbsf depth to mcd is given in tabular form in the site chapter.

Figure 16 illustrates the need for hole-to-hole correlation and the mcd scale. In Figure 16A, color reflectance records from two holes at Site 964 are given on the mbsf depth scale. In Figure 16B, the same records are given after depth scale adjustment. Adjusting the depth scale so that features common to cores in all holes are aligned indicates coring gaps.

The correlation process was iterative. Records of a single physical parameter were moved along a depth scale core by core as correlations between the two holes were made. Although core distortion within a given core was in some cases significant, the core depths were adjusted only by a single constant for each core. The amount of adjustment necessary to optimize the correlation among multiple holes was retained for each core in each hole. The same process was then repeated for the other lithologic parameters to check the core adjustments. Where the amount of offset necessary to align features was ambiguous or uncertain for both lithologic parameters, or where multiple-hole data were unavailable, no depth adjustment for that particular core was made. In these cases, the total amount of offset between mbsf depth and mcd is equal to the cumulative offsets from the overlying cores. Confirmation of the completed composite depth section was provided by comparison with biostratigraphic data from multiple holes.

The composite depth section for each site is presented in tabular format. A portion of the composite depth table for Site 964 is given as an example in Table 3. For each core, the last two columns in Table 3 give the depth offset applied to the ODP sub-bottom depth and the composite depth (mcd). The offset column facilitates conversion of samples that are recorded in ODP sub-bottom depths to composite section depths. By adding the amount of offset listed to the ODP sub-

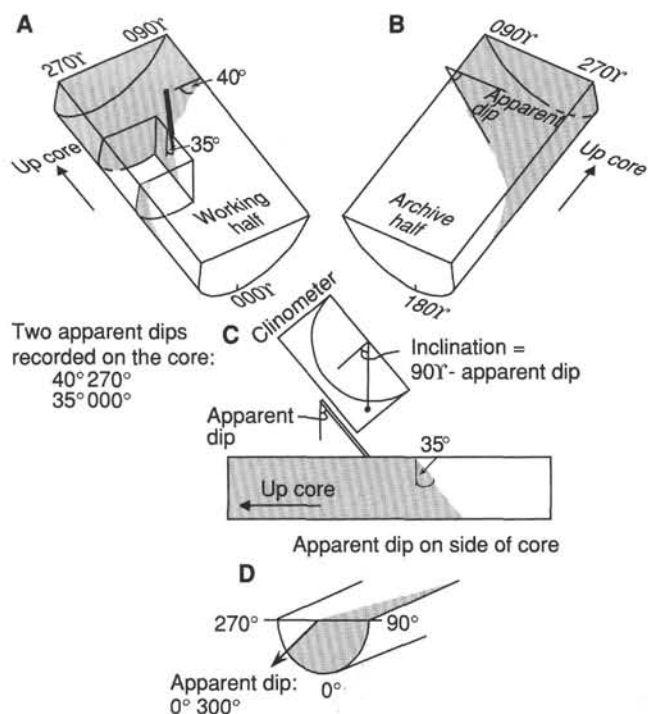


Figure 15. Diagram showing the conventions used in measuring azimuths and dips of structural features in the working and archive halves of cores and the techniques adopted for measuring structural planes in three dimensions in the core reference frame. The east-west (core reference frame) apparent dip of the feature is measured first, generally on the face of the archive half (B). The data are recorded as an apparent dip toward either 90° or 270°. In this case, the apparent dip is toward 270°. A second apparent dip is measured by making a cut parallel to the core axis but perpendicular to the core face in the working half of the core (A). Note that these cuts are normally considerably smaller than that shown in the diagram. The feature is identified on the new surface and the apparent dip in the north-south direction (core reference frame) marked with a toothpick. The apparent dip is measured with the modified protractor (C) and quoted as a value toward either 000° or 180°. In this case, the apparent dip is toward 180° (in the working half). Another possible approach for estimating the second apparent dip requires a cut in the horizontal direction with respect to the core axis (D). In this case, the azimuth represents the direction of a 0°-dip plane. If possible, measurements of both the apparent dip on the core face and two apparent dips are perpendicular to it are used to calculate the true dip and dip direction of the surface in the core reference frame.

bottom depth (mbsf) of a measurement taken in a particular core, the equivalent in mcd is obtained. Thus, the depth conversion table can serve as a sampling strategy guide.

After composite depth construction, a single spliced record representative of the multiple cored sedimentary sequence was assembled. Because the missing intervals of the sedimentary sequence from a single hole could be identified, it was possible to patch missing intervals with data from adjacent holes. The prototype software developed specifically for this application was used to identify tie points for each splice. By identifying the intervals where features present in the multiple holes were most highly correlated, it was possible to construct a spliced record without the danger of mistakenly duplicating any individual features or cycles. Because there is considerable stretching and/or compression of many sections of core relative to the same core in adjacent holes, the precise length of the splice depends on which intervals of core are selected to build it. Tables listing the

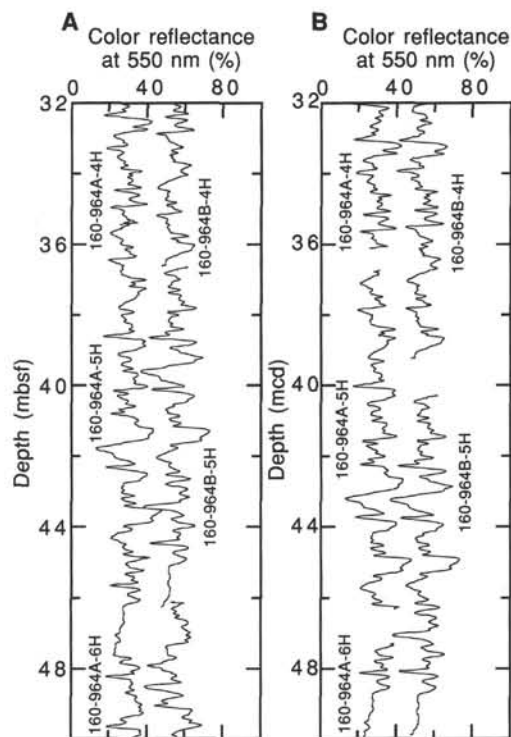


Figure 16. Portions of the color reflectance records from Site 964. A. Cores plotted on the ODP mbsf depth scale. Data from each hole are offset for clarity. B. The same cores on the mcd depth scale. The composite depth section has the advantage that features common to all holes are in relative alignment.

tie points for construction of the spliced record are given in each site chapter.

## INORGANIC GEOCHEMISTRY

### Interstitial-water Sampling and Chemistry

Shipboard interstitial-water analyses were performed on 5- to 10-cm-long whole-round sections that were cut immediately after core retrieval on deck. Samples were usually taken from the bottom of Section 5 of the second and third cores and from each third core thereafter. In addition, three samples were obtained from Sections 1, 3, and 5 of a mud-line core. Interstitial waters were collected using a titanium squeezer (modified after Manheim and Sayles, 1974) and an aluminum squeezer with a nylon liner (Brumsack et al., 1992). Before squeezing, the surface of each whole-round sample was carefully scraped with a spatula to remove potential contamination. After loading the squeezer, pore waters were extruded by applying pressures up to 40,000 lb (approximately 4150 psi) with a hydraulic press. Interstitial-water samples were collected into 50-mL plastic syringes and subsequently filtered through 0.45- $\mu$ m Gelman polysulfone disposable filters. Samples were stored in plastic vials prior to analysis. Aliquots for shore-based analyses were placed in heat-sealed acid-washed plastic tubes and glass ampoules.

Interstitial-water samples were routinely analyzed for salinity as total dissolved solids (g/kg) with a Goldberg optical hand-held refractometer (Reichert) and for pH and alkalinity by Gran titration with a Brinkmann pH electrode and a Metrohm autotitrator. Chloride was analyzed by titration with visual and potentiometric end-point determination; calcium and magnesium concentrations were ana-

Table 3. A portion of the composite depth section for Site 964.

Core	Depth (mbsf)	Offset (m)	Depth (mcd)
<b>160-964A-</b>			
1H	0.00	0.00	0.00
2H	6.8	-0.38	6.42
3H	16.3	-0.31	15.99
4H	25.8	0.68	26.48
5H	45.3	1.41	36.71
6H	44.8	2.47	47.27
7H	54.3	3.61	57.91
8H	63.80	4.87	68.67
9H	73.30	13.14	86.44
10H	82.8	12.50	95.30
11H	92.30	12.97	105.27
<b>160-964B-</b>			
1H	0.00	0.06	0.06
2H	8.10	0.50	8.60
3H	17.60	0.90	18.50
4H	27.10	2.64	29.74
5H	36.60	3.63	40.23
6H	46.10	4.49	50.59
7H	55.60	5.79	61.39
8H	65.10	7.80	72.90
9H	74.60	7.80	82.40
10H	84.10	10.41	94.51
11H	93.60	10.50	104.10
<b>160-964C-</b>			
1H	0.00	0.04	0.04
2H	5.10	3.04	8.14
3H	14.60	3.75	18.35
4H	24.10	5.85	29.95
5H	33.60	6.98	40.58
6H	43.10	8.51	51.61
7H	52.60	9.04	61.64
8H	62.10	8.62	70.72
9H	71.60	8.52	80.12
10H	81.10	13.57	94.67
11H	90.60	13.57	104.17
12X	95.60	13.57	109.17
<b>160-964D-</b>			
1H	0.00	0.06	0.06
2H	4.10	2.86	6.96
3H	13.60	2.75	16.35
4H	23.10	1.54	24.64
5H	32.60	5.59	38.19
6H	42.10	6.37	48.47
7H	51.60	7.11	58.71
8H	61.10	8.34	69.44
9H	70.60	10.32	80.92
10H	80.10	10.29	90.39
11H	89.60	14.17	103.77
12H	99.10	15.59	114.69
<b>160-964E-</b>			
1H	0.00	0.37	0.37
2H	5.50	5.86	11.36
3H	15.00	3.66	18.66
4H	57.00	8.18	65.18
5H	66.50	10.36	76.86
6H	76.00	10.47	86.47
<b>160-964F-</b>			
1H	0.00	0.41	0.41
2H	9.10	1.52	10.62
3H	18.60	2.04	20.64

lyzed by titration; and silica and ammonium were analyzed by spectrophotometric methods with a Milton Roy Spectronic 301 spectrophotometer (Gieskes et al., 1991). International Association of Physical Sciences Organizations (IAPSO) standard seawater was used for calibrating most techniques and for determining accuracy and precision. Standard errors were the following: alkalinity, better than 1.5%; chloride, 0.4%; calcium, better than 1%; magnesium, 0.5%; and silica and ammonia, 4% to 5%. At all sites, sodium was determined using charge-balance calculations where  $\Sigma(\text{cation charge}) = \Sigma(\text{anion charge})$ .

In addition, potassium, magnesium, calcium, sulfate, and bromide were analyzed by ion chromatography using the Dionex DX-100. The standard errors were for potassium, better than 3%; magnesium and calcium, better than 3%; and sulfate and bromide, better than 4%.

Lithium, potassium, sodium, and strontium concentrations were quantified using flame atomic emission and absorption spectrometry (AES) (Varian SpectraAA-20). Lithium and strontium were determined on 1:10 diluted samples and potassium and sodium were determined on 1:200 diluted samples using an air-acetylene (Li, K, Na) or a nitrous oxide-acetylene (Sr) flame. Standards for all flame AES techniques were matched in matrix composition to the samples. The standard errors were better than 1%–2% for lithium, and better than 2%–3% for potassium, sodium, and strontium.

## ORGANIC GEOCHEMISTRY

The following shipboard procedures were applied to measure volatile hydrocarbons, high-molecular-weight hydrocarbons, and long-chain alkenones and to determine the amount of inorganic (carbonate) carbon and the amount and origin of organic matter in the sediments. These procedures were conducted as part of the routine shipboard safety and pollution-prevention requirements and to provide preliminary information for shore-based research.

### Volatile Hydrocarbons

Low-molecular-weight hydrocarbon samples were obtained by two different methods. A standard headspace procedure (Kvenvolden and McDonald, 1986) involved taking about 5 cm<sup>3</sup> of sediment from each core and putting it into a 21.5-cm<sup>3</sup> glass serum vial. The vial was sealed with a septum and a metal crimp cap and heated at 60°C for 30 min. A 5-cm<sup>3</sup> volume of gas from the headspace in the vial was extracted with a glass syringe for analysis by gas chromatography.

A vacutainer method of gas collection (Kvenvolden and McDonald, 1986) was used where gas pockets or expansion voids were visible in the core while it was still in the core liner. A special tool attached to a gas syringe needle and vacutainer was used to penetrate the core liner and collect the gas.

Headspace and vacutainer gas were both routinely analyzed using a Hewlett Packard 5890 II plus gas chromatograph (GC) equipped with a 2.4 m × 0.32 cm stainless-steel column, packed with HaySep S (80–100 mesh), and a flame ionization detector (FID). This instrument measures accurately and rapidly the concentrations of methane, ethane, ethylene, propane, and propylene. Either the vacutainer or the headspace syringe was directly connected to the gas chromatograph via a 1.0-cm<sup>3</sup> sample loop. Helium was used as the carrier gas and the GC oven was kept at 90°C. A Hewlett-Packard 3365 Chemstation was used for data collection and evaluation. Calibration was made by using Scotty IV analyzed gases. Concentrations were measured in ppm.

When the presence of higher concentrations of C<sub>2+</sub> hydrocarbons was suspected, gas samples collected as described before were injected to the Natural Gas Analyzer (NGA), which measures hydrocarbons from methane to hexane. It consists of a Hewlett-Packard 5890 II plus GC equipped with a 60 m × 0.32 mm DB-1 capillary column and an FID. Nonhydrocarbon gases could be analyzed at the same time via a packed column and a thermal conductivity detector (TCD). For hydrocarbon analysis, the GC oven was heated from 80° to 100°C at 8°C/min and then to 200°C at 30°C/min. Carrier gas and computer control were as described before.

### High-molecular-weight Hydrocarbons and Long-chain Alkenones

Bitumen was analyzed in order to obtain indications of the provenance of the sedimentary organic matter. For an estimate of paleo-sea-surface temperature, measurement of the relative abundances of the long-chain di- and triunsaturated alkenones was attempted. Sol-

vent-soluble organic material (bitumen) was obtained from 1–2 g of dried organic-matter-rich sediment (sapropels) by ultrasonic extraction with dichloromethane (+1% methanol) for 30 min. The mixture was filtered through a paper filter and the solvent removed under a stream of nitrogen on a hot plate at 40°C. The total extract was dissolved in a small amount of hexane and filtered over a disposable Pasteur pipette filled with aluminum oxide to remove highly polar components. The solvent was removed from the eluate as described before. The “nonpolar” extractable material still showed a faintly yellow to golden color and, thus, contained compounds commonly considered polar. It was redissolved in 100  $\mu$ L of hexane and then analyzed by gas chromatography on a Hewlett-Packard Model 5890 II plus GC, equipped with a 50 m  $\times$  0.2 mm HP Ultra 1 (cross-linked methyl silicon gum) capillary column (0.11- $\mu$ m film thickness). Operating conditions were as follows: injector, 250°C; detector, 300°C; temperature program, 30°C (3 min), 10°C/min to 220°C, 4°C/min to 300°C (15 min). Usually, 2–3  $\mu$ L were injected in the splitless mode. Identification of *n*-alkanes was based on comparison of retention times with those of authentic standards, whereas alkenones and alkenoates were compared with chromatograms in the published literature (e.g., Brassell et al., 1986; Prahil and Wakeham, 1987; Prell, Niitsuma, et al., 1989).

### Elemental Analysis

One 5-cm<sup>3</sup> sediment sample taken randomly from each core was analyzed for total carbon (TC), carbonate carbon, total organic carbon (TOC), nitrogen, and sulfur. Additional samples were taken from obviously organic-matter-rich sediments (sapropels) and analyzed for the same parameters.

The carbonate carbon content of the samples was determined using a Coulometrics 5011 carbonate carbon analyzer. A sample of about 10 mg of freeze-dried ground material was reacted with 2N HCl in a glass ampoule. The liberated CO<sub>2</sub> is swept into a reaction vessel by a He stream and forms a titratable acid with a blue monothanolamine indicator solution causing the color to fade. The change in color is measured by a photodetector cell that automates a platinum anode to produce base electrically, which in turn returns the indicator to its original color. The amount of current needed is proportional to the amount of CO<sub>2</sub> produced. Carbonate contents are expressed as weight percent CaCO<sub>3</sub>, assuming all the carbonate was present as calcite.

Total carbon, nitrogen, and sulfur were determined using a Carlo Erba 1500 CNS Analyzer. About 5 mg of freeze-dried ground sediment with vanadium pentoxide catalyst added was combusted at 1000°C in a stream of oxygen. Nitrogen oxides were reduced to N<sub>2</sub> and the mixture of SO<sub>2</sub>, CO<sub>2</sub>, and N<sub>2</sub> was separated by gas chromatography and quantified with a TCD. The TOC contents of the sediment samples were determined by calculating the difference between carbonate carbon and the total carbon value.

### Organic Matter Type

The type of organic matter was evaluated by pyrolysis using the Delsi-Nermag Rock-Eval II system. This uses a whole-rock pyrolysis technique to identify the type and maturity of organic matter and to detect the petroleum potential of the sediments (Espitalié et al., 1986). The Rock-Eval system involves a temperature program that first releases volatile hydrocarbons (S<sub>1</sub>) at 300°C for 3 min, and then releases hydrocarbons from the thermal cracking of kerogen (S<sub>2</sub>) as the temperature increases from 300° to 600°C at 25°C/min. S<sub>1</sub> and S<sub>2</sub> hydrocarbons are measured by an FID and reported in milligrams per gram of sediment. The temperature at which the kerogen yields the maximum amount of hydrocarbons during the S<sub>2</sub> program provides T<sub>max</sub> (°C), a parameter that assesses the maturity of the organic matter. Between 300° and 390°C of the pyrolysis program, CO<sub>2</sub> released

from the thermal degradation of organic matter (S<sub>3</sub>) is trapped and measured by a TCD in milligrams per gram of sediment. Rock-Eval II parameters characterize organic matter by allowing the following indexes to be calculated: hydrogen index (HI), (100  $\times$  S<sub>2</sub>)/TOC expressed as mg hydrocarbons/g TOC; oxygen index (OI), (100  $\times$  S<sub>3</sub>)/TOC expressed as mg CO<sub>2</sub>/g TOC; S<sub>2</sub>/S<sub>3</sub> ratio; production index (PI), S<sub>1</sub>/(S<sub>1</sub> + S<sub>2</sub>); and petroleum potential (PC; pyrolyzable carbon), 0.083(S<sub>1</sub> + S<sub>2</sub>). Interpretation of Rock-Eval data is considered unreliable for samples containing less than 0.5% TOC (Peters, 1986). A Hewlett-Packard 3365 Chemstation computer data analysis system was used to integrate and store the results obtained from the Rock-Eval II instrument.

In addition, pyrolysis-gas chromatography was performed using a Geofina Hydrocarbon Meter (GHM). This instrument employs a Varian 3400 GC that has been modified to include a programmable pyrolysis injector. The system has three FIDs and two capillary columns (25 m, GC2 fused silica). Like the Rock-Eval II, this tool determines S<sub>1</sub>, the free hydrocarbons (and similarly volatile compounds) that are released up to 300°C, and S<sub>2</sub>, the pyrolysis products that are generated from the sample kerogen. The effluent of the furnace is split 20:1 so that the hydrocarbon distributions making up S<sub>1</sub> and S<sub>2</sub> can be examined in detail by capillary gas chromatography.

## PHYSICAL PROPERTIES

The principal objectives for the physical properties measurements are (1) to provide high-resolution physical data of the sediments, (2) to determine the effects of sedimentological and textural changes on the physical properties, (3) to calibrate downhole logs, and (4) to constrain the interpretation of seismic reflection data.

Nondestructive high-resolution measurements of whole-round core sections were obtained from the multisensor track, including a gamma-ray attenuation porosity evaluator for estimating wet-bulk density, compressional-wave (*P*-wave) core logger (PWL), magnetic susceptibility meter, and multichannel natural gamma-ray spectrometer.

In unlithified sediment, measurements on the working half of the core included vane shear strength and *P*-wave velocity. In the more lithified sediments, thermal conductivity was measured using a half-space needle probe method, and *P*-wave velocities were determined from cut pieces of the sediment. Throughout the core, index properties (water content, wet- and dry-bulk densities, grain density, porosity, and void ratio) were determined from discrete samples. Some of the dried samples were also used for organic and inorganic geochemical analyses (see “Organic Geochemistry” and “Inorganic Geochemistry” sections, this chapter).

### Multisensor Track

The MST incorporates the magnetic susceptibility meter (MSM), GRAPE, *P*-wave logger, and natural gamma-ray device (NGR). The sampling rate was typically one measurement every 0.5 to 2.5 cm for the GRAPE, 3 to 5 cm for magnetic susceptibility using either the 0.1 or the 1.0 range on the Bartington meter, 30 to 50 cm for natural gamma-ray radiation, and 1.5 to 3.0 cm for *P*-wave velocity.

The GRAPE makes measurements of bulk density at discrete intervals by comparing the attenuation of gamma rays through the cores with attenuation through an aluminum standard (Boyce, 1976). Generally, the GRAPE data are most reliable in APC and nonbiscuited XCB and RCB cores.

The PWL transmits 500-kHz compressional wave pulses through the core at a rate of 1 kHz. The transmitting and receiving transducers are aligned perpendicular to the core axis. A pair of displacement transducers monitors the separation between the compressional wave transducers. Variations in the outside diameter of the liner do not de-

grade the accuracy of the velocities; but the PWL does not provide accurate measurements on cores thinner than the inner diameter of the core liner.

Magnetic susceptibility was measured on all sections at 5-cm intervals using the 0.1 range on the Bartington meter with an 8-cm-diameter loop. The close sampling interval for magnetic susceptibility was chosen to provide another measure for hole-to-hole correlation.

### Thermal Conductivity

The thermal conductivity of whole-core sections was measured using the needle probe method in full-space configuration for soft sediments (von Herzen and Maxwell, 1959). All measurements were made after the cores had equilibrated to the laboratory temperature. Data are reported in units of  $W/(m \cdot K)$ , and have an estimated error of  $\pm 5\%$ – $10\%$ .

Needle probes containing a heating wire and a calibrated thermistor were inserted into the sediment through small holes drilled in the core liners before the sections were split. This system allowed up to four probes to be connected and operated simultaneously.

At the beginning of each test, temperatures in the samples were monitored without applying a heater current until the background thermal drift was determined to be less than  $0.04^\circ C/min$ . Once the samples were equilibrated, the heater circuit was closed and the temperature rise in the probes was recorded. Thermal conductivities were calculated from the rate of temperature rise while the heater current was flowing.

After the heater has been on for about 60 s, the needle probe response is close to that of a line source with constant heat generation per unit length. Temperatures recorded during a time interval of 60–240 s were fit using a least-squares technique to the appropriate equation:

$$T(t) = (q/4\pi k) \cdot \ln(t) + L(t), \quad (1)$$

where  $k$  is the apparent thermal conductivity,  $T$  is temperature,  $t$  is time, and  $q$  is the heat input per unit length of wire per unit time. The term  $L(t)$  describes a linear change in temperature with time, and includes the background temperature drift and any linearity that results from instrumental errors and the geometrical inadequacies of the experiment. These inadequacies include the finite length of the probe and sample.

All full-space measurements were corrected for a linear offset between measured and true thermal conductivities, determined from a series of tests with standards of known conductivities.

### Shear Strength Measurements

The undrained shear strength ( $S_u$ ) of soft cohesive sediments was measured with the Wykeham-Farrance motorized vane shear device following the procedures of Boyce (1976). Measurements were performed at a rate of one per core section to two per whole core. The instrument measures the torque and strain at the vane shaft using a torque transducer and potentiometer, respectively. The shear strength reported is the peak strength determined from the torque vs. strain plot. In more lithified sediments, a Soil Test CL-700 hand-held penetrometer was used.

### P-wave Velocity

In addition to the MST measurements,  $P$ -wave velocity ( $V_p$ ) was determined on discrete samples using three different measurement systems, depending on the degree of sediment lithification. Travel-times were measured in poorly consolidated sediment using a Dalhousie University/Bedford Institute of Oceanography digital sound velocimeter (DSV) (Mayer et al., 1988; Courtney and Mayer, 1993). The velocity calculation is based on the measurement of the travel-

time of an impulsive acoustic signal traveling between a pair of piezoelectric transducers inserted in the split sediment cores. One transducer pair, mounted with a fixed separation (approximately 7.0 cm), is positioned parallel to the core axis (DSV 1); another pair is perpendicular to the core axis (DSV 2). The signal used is a  $0.1\text{-}\mu s$  square wave with a period of 0.2 ms. The received signal was stacked on the rise of the source impulse, resulting in decreased noise and improved detection of the first arrival. The first arrivals were hand picked and the DSV software calculated sediment velocity. The temperature of the unlithified sediments was measured with a digital thermometer probe so that corrections for in situ temperature can be made.

When the material became too consolidated to insert the DSV transducers, measurements were made through the core-barrel liner with the Hamilton Frame system (DSV 3). Typically, there is a measurement gap of about 50 m where the sediment is too consolidated to accommodate the insertion transducers without splitting, but not sufficiently stiff to utilize the Hamilton Frame. The velocity estimate is based on the traveltime between two contact transducers. One is placed on the cut surface of the core. The other is directly beneath, in contact with the core-barrel liner. Sample thickness is usually measured by a vertical offset gauge. Occasional failure of this device makes the use of a hand-held micrometer necessary. The measurements were made along the axis of the core. Fresh water was used to improve the acoustic contact between the sample and the transducers. The source signal for the Hamilton Frame, stacking, and identification of the first arrival are identical as for the insertion transducers described above.

### Index Properties

Index properties (water content, wet- and dry-bulk densities, grain density, porosity, and void ratio) were typically determined from one sample (about  $10\text{--}15\text{ cm}^3$ ) from Sections 2 and 5 of the "A" hole at each site.

The samples were placed in precalibrated aluminum containers prior to weight and volume measurements. Sample weights were determined to a precision of  $\pm 0.005\text{ g}$  using a Scitech electronic balance and a specially designed statistical routine using LabView software. The individual weights were determined with a confidence level of 99.5%; weight was determined from discrete weighings to the point where an additional weight measurement did not change the mean by more than 5%. The mean value calculated from the two determinations was used. Volumes were determined using a helium-displacement Quantachrome Penta-Pycnometer. The pycnometer measures the volume of each sample to a precision of  $\pm 0.04\text{ cm}^3$ . Dry weight and volume measurements were performed after the samples were oven-dried at  $110^\circ C$  for 24 hr and allowed to cool in a desiccator.

Index properties were calculated from measurements of the wet and dry masses of the sample and from the volume using two different methods described in the ASTM designation (D) 2216 (ASTM, 1989). Method B uses the volume of the wet sample, whereas in method C the volume of the dry sample is used. The dry volume is corrected for salt, assuming an interstitial pore-water salinity of 35 (Boyce, 1976). This correction was applied to grain density and porosity computations, as per Hamilton (1971) and Boyce (1976), but not to bulk density.

### SITE GEOPHYSICS

During Leg 160, the Geometrics G801 proton precession magnetometer was not used because the data it provided were so noisy as to be completely unusable. Consequently, the data are not considered significant because the magnetic field of the Mediterranean is generally of little importance with respect to the objectives of Leg 160. Magnetic anomalies in the Eastern Mediterranean are very small and

unconnected to the features studied except for Eratosthenes Seamount, which has a large and rather well-known magnetic anomaly (see "Tectonic Introduction" chapter, this volume).

The seismic system used comprises 80-in.<sup>3</sup> SSI water guns, 200- and 400-in.<sup>3</sup> Amco water guns, and a single-channel, oil-filled Teledyne streamer. The source is towed at a set depth of approximately 10 m and the receiver is towed at a similar depth, although it may be changed slightly. The source is not permitted to be towed closer to the ship for safety reasons. The center of the 100-m active section of the streamer is located about 500 m astern of the ship; the common depth point (CDP) offsets are therefore 300 and 311 m, respectively, for the 80- and 200-in.<sup>3</sup> water guns. On Leg 160, the 80-in.<sup>3</sup> gun was used because there were no deep targets and the higher resolution was considered more important. The data are recorded separately on two analog graphic recorders and by the a2d data-acquisition program. The data digitized by the a2d software are recorded on 4-mm DAT and 8-mm Exabyte tape cartridges and graphically displayed on a Sun work station. The SioSeis seismic processing package, which was developed at Scripps Oceanographic Institution, is used for processing the data and plotting the results on a Versatec plotter. The data may also be imported by software used for creating synthetic seismograms from downhole logging or physical properties measurements, for the purpose of comparison of actual and synthetic profiles at the site.

The seismic data are not of outstanding quality because of the level of noise on the ship and because the source and receiver are old and cannot be deployed in a more flexible manner. Because of the depth of the source, the source pulse is long (about 100 ms) and reverberant with predominantly low frequencies. At ship speeds greater than 6 kt the records become very noisy. The main purpose of the seismic profiling is restricted to confirming the location of the site as specified following the original site survey.

## DOWNHOLE MEASUREMENTS

During Leg 160, the Formation MicroScanner, geological high-sensitivity magnetic tool (GHMT), and geochemical logging tool (GLT) were used by ODP for the first time in the Mediterranean together with standard logging tools. The downhole continuous record of high-resolution microresistivity (FMS), magnetostratigraphy (GHMT), and specific geochemical data (GLT) allowed a precise recognition of structural and sedimentary features.

The Schlumberger MAXIS 500 logging system made the high-resolution logging techniques available to ODP. The Lamont-Doherty Borehole Research Group (LDEO-BRG) in conjunction with Schlumberger Well-Logging Services provided the geophysical logging. All the logging tools are adapted to meet ODP requirements and hole conditions.

During each logging run, incoming data were acquired, archived, and monitored in real time on the MAXIS 500 logging computer. The Cyber Service Unit (CSU) computer was used for the geochemical logging string. After logging, data were transferred to a Sun work station and a Macintosh computer for preliminary shipboard processing and interpretation.

### Logging Tool Strings

Individual logging tools were combined in five different strings (Fig. 17): (1) seismic-stratigraphic tool comprising the natural gamma-ray spectrometry tool (NGT), long-spaced sonic tool (LSS/SDT), phaser dual induction–spherically focused resistivity tool (DIT-SFL), and Lamont-Doherty temperature logging tool (TLT); (2) litho-porosity tool comprising the NGT, compensated neutron porosity tool (CNT), high-temperature lithodensity tool and caliper (HLDT/CALI), and TLT; (3) FMS tool; (4) GLT; and (5) GHMT. The NGT is run on all tool strings to provide a common basis for log

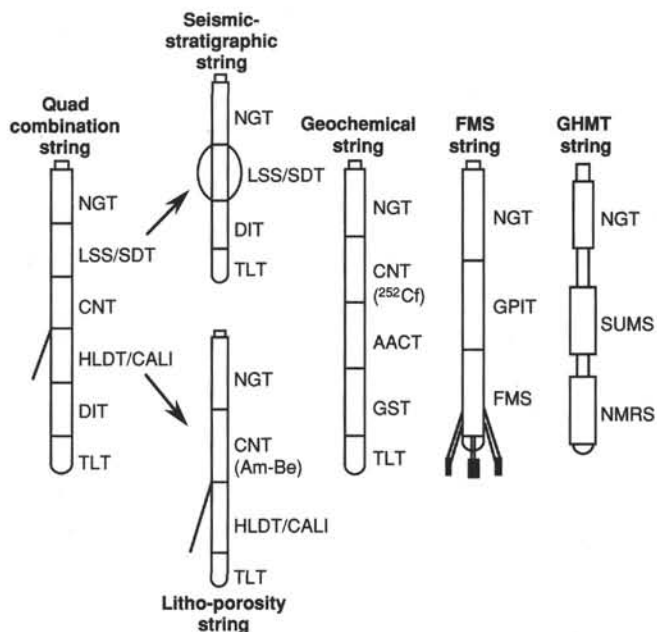


Figure 17. Schematic diagram of the Schlumberger logging tool strings used on Leg 160. Tool strings are not drawn to scale.

correlations. The seismic-stratigraphic and litho-porosity strings can be combined into a single string termed the Quad combination (total length = 31 m).

A brief description of the logging tools employed during Leg 160 is given below. The detailed principles of operation of the various logging sensors can be found in Ellis (1987), Schlumberger (1989), Serra (1984), and Timur and Toksöz (1985).

### Natural Gamma-ray Spectrometry Tool

The NGT measures the natural radioactivity of the formation as both the number of gamma rays and the energy level, which allows us to determine the concentrations of radioactive potassium, thorium, and uranium in the formation (Lock and Hoyer, 1971). The NGT also provides a measure of the total gamma-ray signature (SGR, or K + U + Th) and a uranium-free measurement (CGR, or K + Th). Values are recorded every 0.15 m and have a vertical resolution in the order of 0.46 m. The measurements can be used to estimate the clay content and composition. U/Th ratios from NGT data are used also as organic carbon content indicators and to distinguish changes in the oxidation state of diagenetic minerals.

### Phaser Dual Induction–Spherically Focused Resistivity Tool

The DIT-SFL provides three different measurements of electrical resistivity. Each of these has a different penetration depth into the formation: 1.5 m for the deep induction tool (IDPH), 0.75 m for the medium induction tool (IMPH), and 0.38 m for the shallow spherically focused resistivity signals (SFL). The vertical resolution for the resistivity values are 2 m (IDPH), 1.5 m (IMPH), and 0.75 m (SFL). Values are recorded every 0.15 m.

Resistivity is controlled not only by lithology but also by water content and salinity and is therefore primarily related to the inverse square root of porosity (Archie, 1942). The main factors influencing the resistivity of a formation include the concentration of hydrous and metallic minerals, hydrocarbons and gas hydrates, and pore structure geometry, distribution, and interconnection.

### Long-spaced Sonic Tool and Digital Sonic Tool

The LSS and SDT measure the time required for acoustic waves to travel through the formation between an array of transmitters and receivers separated by vertical distances ranging from 0.91 to 3.66 m. The vertical resolution is in the range of 0.61 m. They provide a direct measurement of acoustic velocity through sediments from the interval transit time measured, and are likely to yield measurements free from the effects of formation damage and enlarged borehole from drilling processes. Sound velocity is related to sediment porosity and lithification and/or compaction. In conjunction with density logs or core physical property measurements, sonic logs are used to compute synthetic seismograms and time depths to seismic reflectors.

### High-temperature Lithodensity Tool

The HLDT provides values of bulk formation density (RHOB), which are dependent on the formation lithology and porosity. The measurements are obtained by means of a radioactive source and two detectors that record an energy spectrum, which is directly related to the number of electrons in the formation. A caliper measurement is made of the borehole diameter to correct the measurements for poor contacts of the detector pads with the borehole wall. The vertical resolution of the measurements is in the order of 0.45 m.

### Compensated Neutron Porosity Tool

Neutron logs are sensitive to lithology and/or porosity. The CNT uses a source that bombards the formation and borehole with fast neutrons at 4.5 MeV and two pairs of sensors that detect the number of neutrons in the epithermal (0.1–100 eV) and thermal (<0.025 eV) energy ranges. The tool's resolution is approximately 0.45 m.

### Geochemical Logging Tool String

The geochemical logging tool is used to determine the concentrations of some major and trace elements, from which lithologic or mineralogical variations can be inferred by comparison with measurements made by X-ray diffraction and fluorescence and core descriptions. It consists of an NGT, CNT (used here as a carrier for a  $^{252}\text{Cf}$  source of neutrons for the aluminum activation clay tool, or AACT; Hertzog et al., 1989), and gamma-ray spectroscopy tool (GST) (Fig. 18).

The GST is located at the base of the string and consists of a high-energy pulsed neutron accelerator (14 MeV) and a NaI scintillation crystal detector. The gamma rays emitted by the nuclei in the formation after neutron capture are detected by the tool sensor. Each element has a characteristic contribution of each of the major elements that dominate the spectrum: Ca, Si, Fe, Cl, H, and S. Calculation of absolute concentrations in weight percent of elemental oxides and rare-earth elements (Gd, Sm, and Ti) requires additional shore-based processing, but relative values may be computed on the ship as concentration ratios. Concentration of Mg and Na may also be obtained by combining the GST data with the logs from the HLDT (photoelectric index).

### Formation MicroScanner Tool String

The FMS string provides high-resolution microresistivity curves from which borehole wall images are produced. FMS data allow continuous high-resolution observation and description of sedimentological and structural features. The FMS tool consists of four orthogonal pads with 16 button electrodes on each pad. Each pad measures about 8 cm<sup>2</sup>, and one pass of the tool covers approximately 30% of a 25.72-cm-diameter borehole, providing a vertical resolution of approximately 0.5 cm at a sampling interval of 0.25 cm (Serra, 1989). The

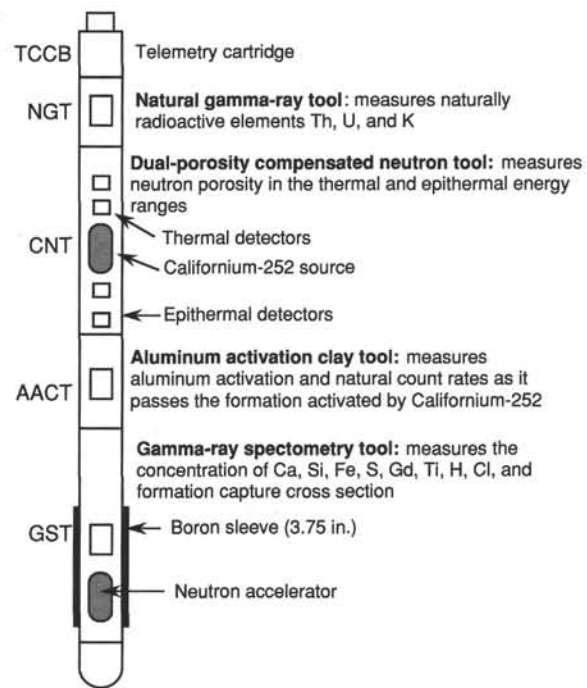


Figure 18. Schematic drawing of the Schlumberger geochemical logging tool string run in Hole 967E.

FMS tool string contains a general purpose inclinometry tool (GPIT) that orients the resistivity measurements through the use of an accelerometer and magnetometer that respond to the declination and inclination of the Earth's magnetic field so that the orientation of the interpreted sedimentary or structural features with respect to geographical coordinates can be easily determined. It is also used to determine the orientation of cores and core-derived data.

### Geological High-sensitivity Magnetic Tool String

The geological high-sensitivity magnetic tool string comprises a high-sensitivity total magnetic field sensor (NMRS) coupled with a magnetic susceptibility sensor (susceptibility magnetic sonde, or SUMS), which are used to detect borehole magnetic polarity transitions and susceptibility variations, respectively. The NMRS measures the frequency of proton precession between a calibrated applied polarizing field and the Earth's magnetic field that is proportional to the total field intensity of the earth. An average precision of 0.5 nT is based on duplicate runs. Its sensitivity is about  $10^{-2}$  nT. The SUMS measures mutual inductance caused by the surrounding borehole lithology using a transmitter coil and a receiver coil separated as a two-coil induction sonde. The precision between duplicate runs is generally better than  $3 \times 10^{-6}$  SI and the sensitivity of the sonde is almost  $10^{-6}$  units. Data are recorded every 5 cm.

Specifications of the probes, such as impulse response, calibration ratio, and geomagnetic location of the hole, are used to calculate the susceptibility effect on the scalar total-field magnetometer. From these data the scalar remanent magnetization can be calculated.

### Lamont-Doherty Temperature Logging Tool

The LDEO TLT is a high-precision, low-temperature logging tool. It is self-contained and provides a series of accurate temperature logs while keeping total logging time the same. Data from two thermistors and a pressure transducer are collected every 1 s and are re-

corded internally. Once the in situ measurement is completed, the data are transferred to a shipboard computer for analysis. The TLT measures the borehole water temperature rather than the true formation temperature; it is common to observe gradual borehole warming (thermal rebound) as logging proceeds.

### Shore-based Log Processing

Processing, quality control, and display of the logging data were performed for each of the seven logged sites by LDEO-BRG, the Leicester University Borehole Research Group (LUBR), and the Institut Méditerranéen de Technologie, using Schlumberger Logos software and additional programs developed by members of the BRG. Displays of most of these processed data appear with accompanying text at the end of the appropriate site chapters in this volume. Files of all processed logs (including FMS, dipmeter, BRG temperature data, high-resolution density and neutron data, and sonic waveforms not shown in printed form) and explanatory text are included on the CD-ROM in the back pocket of this volume; the directory of the contents of the CD-ROM is at the front of this volume.

Shore-based processing of data from each hole consisted of (1) depth adjustments of all logs to a common measurement below the seafloor, (2) corrections specific to certain tools, and (3) quality control and rejection of unrealistic values.

The depth-shifting procedure is based on an interactive, graphical depth-match program that allows the processor to visually correlate logs and define appropriate shifts. The reference log and the log to be adjusted in depth are displayed side-by-side on a screen, and vectors connect the two at positions chosen by the user. The total gamma-ray curve (SGR) from the NGT tool run on each logging string was used in most cases to correlate the logging runs. In general, the reference curve is chosen on the basis of constant, low cable tension and high cable speed (tools run at faster speeds are less likely to stick and are less susceptible to data degradation caused by ship heave). Other factors, however, such as the length of the logged interval, the presence of drill pipe, and the statistical quality of the collected data (better statistics are obtained at lower logging speeds) are also considered in the selection. A list of the amount of differential depth shifts applied at each hole is available upon request to LDEO-BRG.

Specific tool corrections were performed on the gamma-ray data to account for changes in borehole size and for the composition of the drilling fluid. Processing techniques unique to the AACT and GST tools of the geochemical string are described in detail below.

Quality control was performed by cross correlation of all logging data. If the data processor concluded that individual log measurements represented unrealistic values, the choices were to either discard the data outright and substitute the null value of “-999.25” or identify a specific depth interval containing suspect values that must be used with caution. The latter are noted in the text that accompanies all processed log displays. Quality control of the acoustic data was based on discarding any of the four independent transit-time measurements that were negative or that fell outside a range of reasonable values selected by the processor.

In addition to the standard 15.24-cm sampling rate, bulk density and neutron data were recorded at sampling rates of 2.54 and 5.08 cm, respectively. The enhanced bulk-density curve is the result of a Schlumberger enhanced processing technique performed on the MAXIS system on board. While in normal processing short-spacing data is smoothed to match the long-spacing one, in enhanced processing this is reversed. In a situation where there is good contact between the HLDT pad and the borehole wall (low density correction) the results are improved, because the short-spacing data have a better vertical resolution.

Locally, some intervals of log data appeared unreliable (usually owing to poor hole conditions) and were not processed beyond what had been done aboard ship. In general, a large (>12 in.) and/or irreg-

ular borehole affects most recordings, particularly those that require eccentricization (HLDT) and a good contact with the borehole wall. Hole deviation can also degrade the data; the FMS, for example, is not designed to be run in holes that are more than 10° off the vertical, as the tool weight might cause the caliper to close.

### Geochemical Tool String<sup>3</sup>

The geochemical logging tool string consists of four separate logging tools: the NGT, CNT, AACT, and GST. A schematic drawing of the GLT, which was run in Hole 967E on Leg 160, is shown in Figure 18. These four tools use three separate modes of gamma-ray spectroscopy for a comprehensive elemental analysis of the formation. The NGT is located at the top of the tool string so that it can measure the naturally occurring radionuclides thorium, uranium, and potassium before the formation is irradiated by the nuclear sources contained in the lower tools (Fig. 18). The CNT, located below the NGT, carries a californium (<sup>252</sup>Cf) neutron source to activate the Al atoms in the formation. The AACT, a modified NGT, is located below the <sup>252</sup>Cf source and measures the activated gamma rays in the formation. By combining the AACT measurement with the previous NGT measurement, the background radiation is subtracted out and a reading of formation Al is obtained (Scott and Smith, 1973). The gamma-ray spectrometry tool, at the base of the string, carries a pulsed neutron generator to induce prompt-capture gamma-ray reactions in the borehole and formation and an NaI(Tl) scintillation detector to measure the energy spectrum of gamma rays generated by the prompt neutron-capture reactions. As each of the elements in the formation is characterized by a unique spectral signature, it is possible to derive the contribution (or yield) of each of the major elements silicon, iron, calcium, titanium, sulfur, gadolinium, and potassium from the measured spectrum and, in turn, to estimate the relative abundance of each in the formation when combined with the elemental concentrations from the NGT and AACT (Hertzog et al., 1989). The GST also measures the hydrogen and chlorine in the borehole and formation, although these elements are not directly used for determining the rock geochemistry.

The only major rock-forming elements not measured by the geochemical tool string are magnesium and sodium; the neutron-capture cross sections of these elements are too small relative to their typical abundances for the GLT to detect. A rough estimate of Mg + Na can be made in some instances by using the photoelectric factor (PEF), measured by the lithodensity tool (Hertzog et al., 1989). This calculation was not implemented on the geochemical data from Hole 967E as the (Mg + Na) component was generally below the detection resolution of this technique (Pratson et al., 1993).

### Data Reduction

The well-log data from the Schlumberger geochemical tools are transmitted digitally up a wireline and are recorded and processed on *JOIDES Resolution* in the Schlumberger CSU. The results from the CSU are made available as “field logs” for initial, shipboard interpretation. Subsequent reprocessing is necessary to correct the data for the effects of fluids added to the well, logging speed, and drill-pipe interference. Processing of the spectrometry data is required to transform the relative elemental yields into oxide weight fractions.

The processing is performed with a set of log-interpretation programs written by Schlumberger that have been slightly modified to account for the lithologies and hole conditions in the ODP holes. The processing steps for the Hole 967E logs are summarized below.

<sup>3</sup>James F. Bristow, Lee Ewert, and Peter K. Harvey, Borehole Research, Department of Geology, University of Leicester, Leicester, LE1 7RH, United Kingdom.

### Step 1: Reconstruction of Relative Elemental Yields from Recorded Spectral Data

This first processing step compares the measured spectra from the gamma-ray spectrometry tool with a series of "standard" spectra to determine the relative contribution (or yield) of each element. These "standards" approximate the spectrum of each element. Using a weighted, least-squares inversion method, the relative elemental yields are calculated at each depth level.

Six elemental standards (Si, Fe, Ca, S, Cl, and H) are used to produce the shipboard yields, but three additional standards (Ti, Gd, and K) can be included in the post-cruise processing to improve the fit of the spectral standards to the measured spectra (Grau and Schweitzer, 1989). The ability to detect an element depends principally on the size of its capture cross section and its abundance in the formation. Although Ti, Gd, and K commonly appear in the formation in very low concentrations, they can make a significant contribution to the measured spectra because they have large neutron-capture cross sections. Gd for example, has a capture cross section of 49,000 barns, whereas that of Si is 0.16 barns (Hertzog et al., 1989). Therefore, including Gd is necessary when calculating the best fit of the standard spectra to the measured spectrum, even though its typical concentration is only a few ppm.

The elemental standards (Si, Ca, Fe, Ti, Gd, S, Cl, and H) were used in the spectral analysis step for Hole 967E. The spectral standard for K was not used in the final analysis because its inclusion in the spectral inversion was found to increase the noise level in the other elemental yields. This was due primarily to the fact that the carbonate sequence in the logged sequence of this hole had a low K concentration. A linear 10-point (5 ft, 1.52 m) moving average was applied to the output elemental yields to increase the signal to noise ratios.

### Step 2: Depth Shifting

Geochemical processing involves the integration of data from the different tool strings; consequently, it is important that all the data are depth-correlated to one reference logging run. The NGT, run on each of the logging tool strings, provides a spectral gamma-ray curve with which to correlate each of the logging runs. A reference run is chosen on the bases of constant and low cable tension and high cable speed (tools run at faster speeds are less likely to stick and are less susceptible to data degradation caused by ship heave). The depth-shifting procedure involves picking a number of reference points based on similar log character and then invoking a program that expands and compresses the matching logging run to fit the reference logging run. The main run of the Quad combination tool string was chosen as the reference run for Hole 967E.

### Step 3: Calculation of Total Radioactivity and Th, U, and K Concentrations

The third processing routine calculates the total natural gamma-ray radiation in the formation, as well as concentrations of Th, U, and K, using the counts in five spectral windows from the NGT (Lock and Hoyer, 1971). This routine resembles shipboard processing; however, the results are improved during post-cruise processing by including corrections for hole-size changes and temperature variations. A Kalman filtering (Ruckebusch, 1983) is used in the CSU processing at sea to minimize the statistical uncertainties in the logs, which can otherwise create erroneous negative values and anticorrelations (especially between Th and U). An alpha filter has been introduced more recently and is now recommended by Schlumberger for shore-based processing. This filter strongly smooths the raw spectral counts but keeps the total gamma-ray curve unsmoothed before calculating out the Th, U, and K. The outputs of this program are K (wet wt%), U (ppm), and Th (ppm), as well as total gamma-ray and computed gamma-ray (total gamma ray minus U contribution). They are displayed as a function of depth in the log summary figures at the end of the relevant site chapter.

### Step 4: Calculation of Al Concentration

The fourth processing routine (PREACT) calculates the concentration of Al in the formation using recorded gamma-ray data from four energy windows on the AACT. During this step, corrections are made for natural radioactivity, borehole-fluid neutron-capture cross section, formation neutron-capture cross section, formation slowing-down length, and borehole size.

Porosity and density logs are needed as inputs into this routine to convert the wet-weight percentages of K and Al curves to dry-weight percentages. To derive the best porosity log, shipboard core porosity measurements were compared with porosity logs calculated from the resistivity (using the relationship of Archie, 1942) and bulk density logs, and taken from the neutron porosity tool. The best correlation with core was found with the neutron porosity log, and this was smoothed by a 5-ft (1.52 m) running average and used in the PREACT routine. The bulk density log used as input into PREACT was edited to remove extremely low values caused by borehole washouts over the interval 70–134 mbsf and at 200, 243, and 276 mbsf.

A correction is also made for Si interference with Al; the  $^{252}\text{Cf}$  source activates Si, producing the aluminum isotope  $^{28}\text{Al}$  (Hertzog et al., 1989). The program uses the Si yield from the GST to determine the Si background correction. The program outputs dry-weight percentages of Al and K, which are combined in the next processing step with the GST-derived elemental yields in the oxide closure model.

### Step 5: Normalization of Elemental Yields from the GST to Calculate the Elemental Weight Fractions

Relative concentrations of the GST-derived elemental yields can be determined by dividing each elemental yield by a relative spectral sensitivity factor ( $S_i$ ). This factor is related principally to the thermal neutron-capture cross sections and also to its gamma-ray production and detection probability of each element (Hertzog et al., 1989). The relative elemental concentrations are related to the desired absolute concentrations by a depth-dependent normalization factor ( $F$ ), as defined by the relationship:

$$Wt_i = FY_i/S_i \quad (2)$$

where  $Wt_i$  = absolute elemental concentration and  $Y_i$  = relative elemental yield.

The normalization factor is calculated on the basis that the sum of all the elemental weight fractions is unity (100%). The closure model handles the absence of carbon and oxygen, which are not measured by this tool string, with the approximation that each of the measurable elements combines with a known oxide or carbonate. The dry-weight percentages of Al and K are normalized with the reconstructed elemental yields to determine the normalization factor at each depth interval from the following equation:

$$F(\sum_i X_i Y_i / S_i) + X_k Wt_k + X_{Al} Wt_{Al} = 100, \quad (3)$$

where  $X_i$  = oxide factor (atomic weight of the associated oxide or carbonate of element  $i$  + atomic weight of element  $i$ ),  $X_k$  = oxide factor (atomic weight  $\text{K}_2\text{O}$  + atomic weight of K),  $Wt_k$  = dry wt% of K as determined from the NGT,  $X_{Al}$  = oxide factor (atomic weight of  $\text{Al}_2\text{O}_3$  + atomic weight of Al), and  $Wt_{Al}$  = dry wt% of Al, as determined from the AACT.

The value of  $X_i$  accounts for the C and O associated with each element. Table 4 lists the oxide factors used in this calculation for Hole 967E.

### Step 6: Calculation of Oxide Percentages

This routine converts the elemental weight percentages into oxide percentages by multiplying each by its associated oxide factor, as shown in Table 4. The results are displayed as a function of depth in the log summary figures at the end of the relevant site chapter.

**Table 4. Oxide factors used in normalizing elements to 100% and converting elements to oxides.**

Element	Oxide/ carbonate	Conversion factor
Si	SiO <sub>2</sub>	2.139
Ca	CaCO <sub>3</sub>	2.497
Fe	FeO*	1.358
K	K <sub>2</sub> O	1.205
Ti	TiO <sub>2</sub>	1.668
Al	Al <sub>2</sub> O <sub>3</sub>	1.889

Note: Total iron as FeO\*.

#### Step 7: Calculation of Error Logs

The statistical uncertainty of each element is calculated for each of the elements measured with the GST and NGT (Grau et al., 1990; Schweitzer et al., 1988; Bristow et al., 1994). This error is strongly related to the normalization factor, which is calculated at each depth level (equation 3). The normalization factor is displayed to the right of the logs in the log summary figures at the end of the relevant site chapter. A lower normalization factor represents better counting statistics and therefore higher quality data.

### IN SITU TEMPERATURE MEASUREMENTS

In situ temperature measurements are of importance to the objectives of ODP Leg 160 because they provide information on the present-day and recent tectonics. Temperature gradients and heat flow were determined from measurements with the ADARA temperature tool used with the APC. Additionally, downhole measurements with the Lamont-Doherty temperature logging tool (see "Downhole Measurements" section, this chapter) were included in heat-flow analyses as the only available data after the refusal of APC coring.

#### ADARA Temperature Tool Measurements

The ADARA coring shoe was used to obtain in situ sediment temperatures during regular piston-coring operations. The instrument contains an electronics section, composed of three circuit boards and two battery packs, built into a cylindrical frame. These components of the thermal tool fit inside an annular cavity of a special APC coring shoe. Two steel prongs extend from the base of the frame and anchor the electronics in place inside the shoe. Inside one of the two prongs is a platinum resistance-temperature device (RTD), which is calibrated over a range of -20°C to 100°C, with resolution of 0.01°C. The platinum sensor records temperature measurements during coring. The tool is programmed after it has been inserted into the coring shoe, and repeated deployments can be run without removing the tool or batteries. After programming and starting the test sequence, a cross-over subassembly with O-rings seals the cavity containing the electronics.

In operation, the coring shoe is mounted on a core barrel and lowered down the pipe by wireline. The tool is typically held for 5–10 min at the mud line to equilibrate with bottom temperatures, and then is lowered to the end of the drill string. Standard APC coring techniques are used, with the core barrel fired out through the drill bit using hydraulic pressure. The tool is then left in place for 10 min instead of being retrieved immediately, so that the tool can begin thermal equilibration with the formation. On Leg 160, the ADARA tool was used to collect temperature measurements at 5-s intervals over a 15-min period. This provided a sufficiently long transient record for reliable extrapolation of the steady-state temperature. Processing of the temperature measurements is described below. The nominal accuracy of the unreduced temperature measurements is estimated to be 0.1°C.

### Data Reduction

The data reduction method estimates the steady-state bottom-hole temperature by forward modeling the recorded transient temperature curve as a function of time. The shape of the transient temperature curve is determined by the response function of the tool and the thermal properties of the bottom-hole sediments (Bullard, 1954; Horai and Von Herzen, 1985). Synthetic curves are constructed, based on tool geometry, sampling interval, and the thermal properties of the tools and surrounding sediments. Thermal time constants are several minutes under normal conditions, requiring that the probe be kept on bottom for at least 10–15 min in order to allow extrapolation of the temperature curves with confidence. In general, the temperature increases immediately following emplacement of the probe, as a result of frictional heating of the probe tip during insertion. The temperature peaks after a short period of time and decreases thereafter, approaching the steady-state temperature of the sediments at a rate inversely proportional to time.

The theoretical decay curves simulate the instantaneous heating (or cooling) of the sediment following probe penetration, but in practice, a finite time is required for the sensors to reach a maximum temperature. As a result, the effective origin time of the thermal pulse is delayed as a function of the tool and sediment properties. In addition, the recorders sample temperatures at fixed intervals, leaving the exact penetration time uncertain. An effective penetration time and an extrapolated temperature are estimated by shifting the time axis of the theoretical thermal decay curves to fit the actual data. Temperatures from the first 5–10 measurements (20–50 s) following penetration commonly do not follow the theoretical curves, but later parts of the records usually provide a very good match (for more details, see "Explanatory Notes" chapter, Leg 155 *Initial Reports* volume; Flood, Piper, Klaus, et al., 1995). The choice of which data should be included in the matching, and which time shift should be used, is partly subjective; it is best to use as much of the actual decay curve as possible. The variations in extrapolated temperatures that result from choosing different time intervals and time shifts can be used to estimate errors associated with the temperatures finally assigned to represent in situ conditions.

Data reduction software developed by ODP was used on Leg 160 to model the transient temperature curve interactively and extrapolate for the equilibrium temperature. Variables in the modeling method are the thermal conductivity of the sediments (based on physical property measurements), tool insertion time, delay time between tool insertion and peak temperature, and the length of the portion of the curve to be fitted. In practice, relatively few iterations of the modeling procedure were required to obtain reasonable fits to the temperature data. The thermal conductivity measurements obtained as part of the routine physical properties analysis were consistent with the modeling and produced reliable equilibrium temperatures. If laboratory thermal conductivity measurements were not available at a site, regional approximations were used.

### REFERENCES

- Archie, G.E., 1942. The electrical resistivity log as an aid in determining some reservoir characteristics. *J. Pet. Technol.*, 5:1–8.
- ASTM, 1989. Annual book of ASTM standards for soil and rock, building stones, geotextiles, (Vol. 04.08):168–862, Philadelphia (Am. Soc. Testing Materials).
- Blow, W.H., 1979. *The Cainozoic Globigerinida*: Leiden (E.J. Brill).
- Boyce, R.E., 1976. Definitions and laboratory techniques of compressional sound velocity parameters and wet-water content, wet-bulk density, and porosity parameters by gravimetric and gamma-ray attenuation techniques. In Schlanger, S.O., Jackson, E.D., et al., *Init. Repts. DSDP*, 33: Washington (U.S. Govt. Printing Office), 931–958.
- Brassell, S.C., Eglinton, G., Marlowe, I.T., Pflaumann, U., and Sarnthein, M., 1986. Molecular stratigraphy: a new tool for climatic assessment. *Nature*, 320:129–133.

- Bristow, J.F., Lofts, J.C., Harvey, P.K., and Lovell, M.A., 1995. Reservoir characterisation using nuclear geochemical logging. *Trans. 4th Int. Congr. Brazilian Geophys. Soc. and 1st Latin Am. Geophys. Conf.*, Rio de Janeiro, 2:723–726.
- Brumsack, H.-J., Zuleger, E., Gohn, E., and Murray, R.W., 1992. Stable and radiogenic isotopes in pore waters from Leg 127, Japan Sea. In Pisciotto, K.A., Ingle, J.C., Jr., von Breyman, M.T., Barron, J., et al., *Proc. ODP, Sci. Results*, 127/128 (Pt. 1): College Station, TX (Ocean Drilling Program), 635–650.
- Bullard, E.C., 1954. The flow of heat through the floor of the Atlantic Ocean. *Proc. R. Soc. London A*, 222:408–429.
- Cande, S.C., and Kent, D.V., 1992. A new geomagnetic polarity time scale for the Late Cretaceous and Cenozoic. *J. Geophys. Res.*, 97:13917–13951.
- , 1995. Revised calibration of the geomagnetic polarity time scale for the Late Cretaceous and Cenozoic. *J. Geophys. Res.*, 100:6093–6095.
- Cita, M.B., 1975. Studi sul Pliocene e gli strati di passaggi dal Miocene al Pliocene, VII. Planktonic foraminiferal biozonation of the Mediterranean Pliocene deep sea record: a revision. *Riv. Ital. Paleontol. Stratigr.*, 81:527–544.
- Cita, M.B., and Castradori, D., 1995. Rapporto sul workshop “Marine sections from the Gulf of Taranto (Southern Italy) useable as potential stratotypes for the GSSP of the Lower, Middle, and Upper Pleistocene” (29 settembre–4 ottobre 1994). *Boll. Soc. Geol. Ital.*, 114:319–336.
- Cita, M.B., Rio, D., and Sprovieri, R., in press. The Pliocene series: chronology of the type Mediterranean record and standard chronostratigraphy. In Wrenn et al. (Eds.), *AASP Spec. Vol.* (Baton Rouge).
- Courtney, R.C., and Mayer, L.A., 1993. Calculating acoustic parameter by a filter correlation method. *J. Acous. Soc. Am.*, 93:1145–1154.
- Curry, W.B., Shackleton, N.J., Richter, C., et al., 1995. *Proc. ODP, Init. Repts.*, 154: College Station, TX (Ocean Drilling Program).
- Ellis, D.V., 1987. *Well Logging For Earth Scientists*: New York (Elsevier).
- Erba, E., Premoli Silva, I., Wilson, P., Pringle, M.S., Silter, W.V., Watkins, D.K., Arnaud Vanneau, A., Bralower, T.I., Budd, A.F., Camoin, G.F., Masse, J.-P., Mutterlose, J., and Sager, W.V., in press. Synthesis of stratigraphies from shallow-water sequence at Sites 871 through 879 in the Western Pacific Ocean (Leg 44). In Haggerty, J.A., Premoli Silva, I., Rack, F., and McNutt, M. (Eds.), *Proc. ODP, Sci. Results*, 144: College Station, TX (Ocean Drilling Program).
- Espalié, J., Deroo, G., and Marquis, F., 1986. La pyrolyse Rock-Eval et ses applications, Partie III. *Rev. Inst. Fr. Pet.*, 41:73–89.
- Flood, R.D., Piper, D.J.W., Klaus, A., et al., 1995. *Proc. ODP, Init. Repts.*, 155: College Station, TX (Ocean Drilling Program).
- Fornaciari, E., and Rio, D., in press. Latest Oligocene to early middle Miocene quantitative calcareous nannofossil biostratigraphy in the Mediterranean region. *Micropaleontology*.
- Fornaciari, E., Di Stefano, A., Rio, D. and Negri, A., in press. Middle Miocene quantitative calcareous nannofossil biostratigraphy in the Mediterranean region. *Micropaleontology*.
- Gieskes, J.M., Gamot, T., and Brumsack, H., 1991. Chemical methods for interstitial water analysis aboard *JOIDES Resolution*. *ODP Tech. Note*, 15.
- Gradstein, F.M., Agterberg, F.P., Ogg, J.G., Hardenbol, J., van Veen, P., Thier, J., and Huang, Z., 1994. A Mesozoic time scale. *J. Geophys. Res.*, 99:24051–24074.
- Grau, J.A., and Schweitzer, J.S., 1989. Elemental concentrations from thermal neutron capture gamma-ray spectra in geological formations. *Nucl. Geophys.*, 3:1–9.
- Grau, J.A., Schweitzer, J.S., and Hertzog, R.C., 1990. Statistical uncertainties of elemental concentrations extracted from neutron-induced gamma-ray measurements. *IEEE Trans. Nucl. Sci.*, 37:2175–2178.
- Hagelberg, T., Shackleton, N., Pisias, N., and Shipboard Scientific Party, 1992. Development of composite depth sections for Sites 844 through 854. In Mayer, L., Pisias, N., Janacek, T., et al., *Proc. ODP, Init. Repts.*, 138 (Pt. 1): College Station, TX (Ocean Drilling Program), 79–85.
- Hamilton, E.L., 1971. Elastic properties of marine sediments. *J. Geophys. Res.*, 76:579–604.
- Hasegawa, S., Sprovieri, R., and Poluzzi, A., 1990. Quantitative analysis of benthic foraminiferal assemblages from Plio-Pleistocene sequences in the Tyrrhenian Sea, ODP Leg 107. In Kastens, K.A., Mascle, J., et al., *Proc. ODP, Sci. Results*, 107: College Station, TX (Ocean Drilling Program), 461–478.
- Hemleben, C., Muhlen, D., Olsson, R.K., and Berggren, W.A., 1991. Surface texture and the first occurrence of spines in planktonic foraminifera from the early Tertiary. *Geol. Jahrb.*, 128:117–146.
- Hemleben, C., Spindler, M., and Anderson, O.R., 1989. *Modern Planktonic Foraminifera*: Berlin (Springer-Verlag).
- Hertzog, R.C., Colson, J.L., Seeman, B., O'Brien, M.S., Scott, H.D., McKeon, D.C., Wraight, P.D., Grau, J.A., Ellis, D.V., Schweitzer, J.S., and Herron, M.M., 1989. Geochemical logging with spectrometry tools. *SPE Form. Eval.*, 4:153–162.
- Hilgen, F.J., 1991a. Astronomical calibration of Gauss to Matuyama sapropels in the Mediterranean and implication for the geomagnetic polarity time scale. *Earth Planet. Sci. Lett.*, 104:226–244.
- , 1991b. Extension of the astronomically calibrated (polarity) time scale to the Miocene/Pliocene boundary. *Earth Planet. Sci. Lett.*, 107:349–368.
- Horai, K., and Von Herzen, R.P., 1985. Measurement of heat flow on Leg 86 of the Deep Sea Drilling Project. In Heath, G.R., Burckle, L.H., et al., *Init. Repts. DSDP*, 86: Washington (U.S. Govt. Printing Office), 759–777.
- Iaccarino, S., 1985. Mediterranean Miocene and Pliocene planktic foraminifera. In Bolli, H.M., Saunders, J.B., and Perch-Nielsen, K. (Eds.), *Plankton Stratigraphy*: Cambridge (Cambridge Univ. Press), 283–314.
- Kidd, R.B., Cita, M.B., and Ryan, W.B.F., 1978. Stratigraphy of eastern Mediterranean sapropel sequences recovered during DSDP Leg 42A and their paleoenvironmental significance. In Hsü, K.J., Montadert, L., et al., *Init. Repts. DSDP*, 42 (Pt. 1): Washington (U.S. Govt. Printing Office), 421–443.
- Kvenvolden, K.A., and McDonald, T.J., 1986. Organic geochemistry on the *JOIDES Resolution*—an assay. *ODP Tech. Note*, 6.
- Larsen, H.C., Saunders, A.D., Clift, P.D., et al., 1994. *Proc. ODP, Init. Repts.*, 152: College Station, TX (Ocean Drilling Program).
- Lock, G.A., and Hoyer, W.A., 1971. Natural gamma-ray spectral logging. *Log Analyst*, 12:3–9.
- MacLeod, C.J., Parson, L.M., and Sager, W.W., 1994. Reorientation of cores using the Formation MicroScanner and Borehole Televiewer: application to structural and paleomagnetic studies with the Ocean Drilling Program. In Hawkins, J., Parson, L., Allan, J., et al., *Proc. ODP, Sci. Results*, 135: College Station, TX (Ocean Drilling Program), 301–311.
- MacLeod, C.J., Parson, L.M., Sager, W.W., and the ODP Leg 135 Scientific Party, 1992. Identification of tectonic rotations in boreholes by the integration of core information with Formation MicroScanner and Borehole Televiewer images. In Hurst, A., Griffiths, C.M., and Worthington, P.F. (Eds.), *Geological Applications of Wireline Logs II*. Geol. Soc. Spec. Publ. London, 65:235–246.
- Manheim, F.T., and Sayles, F.L., 1974. Composition and origin of interstitial waters of marine sediments based on deep sea drill cores. In Goldberg, E.D. (Ed.), *The Sea* (Vol. 5): New York (Wiley Interscience), 527–568.
- Martini, E., 1971. Standard Tertiary and Quaternary calcareous nannoplankton zonation. In Farinacci, A. (Ed.), *Proc. 2nd Int. Conf. Planktonic Microfossils Roma*: Rome (Ed. Tecnosci.), 2:739–785.
- Mayer, L.A., Courtney, R.C., and Moran, K., 1988. Ultrasonic measurements of marine sediment properties. *Prog. Oceanogr.*, 87:1–139.
- Mazzullo, J.M., Meyer, A., and Kidd, R.B., 1988. New sediment classification scheme for the Ocean Drilling Program. In Mazzullo, J., and Graham, A.G., *Handbook for Shipboard Sedimentologists*. ODP Tech. Note, 8:45–67.
- Okada, H., and Bukry, D., 1980. Supplementary modification and introduction of code numbers to the low-latitude coccolith biostratigraphic zonation (Bukry, 1973; 1975). *Mar. Micropaleontol.*, 5:321–325.
- Peters, K.E., 1986. Guidelines for evaluating petroleum source rock using programmed pyrolysis. *AAPG Bull.*, 70:318–329.
- Prahl, F.G., and Wakeham, S.G., 1987. Calibration of unsaturation patterns in long-chain ketone compositions for paleotemperature assessment. *Nature*, 330:367–369.
- Pratson, E.L., Broglia, C., and Jarrard, R., 1993. Data report: geochemical well logs through Cenozoic and Quaternary sediments from Sites 815, 817, 820, 822, and 823. In McKenzie, J.A., Davies, P.J., Palmer-Julson, A., et al., *Proc. ODP, Sci. Results*, 133: College Station, TX (Ocean Drilling Program), 795–817.
- Prell, W.L., Niitsuma, N., et al., 1989. *Proc. ODP, Init. Repts.*, 117: College Station, TX (Ocean Drilling Program).
- Premoli Silva, I., and Boersma, A., 1989. Atlantic Paleogene planktonic foraminiferal bioprovincial indices. *Mar. Micropaleontol.*, 14:357–371.
- Premoli Silva, I., and Sliter, W.V., 1994. Cretaceous planktonic foraminiferal biostratigraphy and evolutionary trends from the Bottaccione Section, Gubbio, Italy. *Palaeontogr. Ital.*, 82:2–90.
- Rio, D., Raffi, I., and Villa, G., 1990. Pliocene-Pleistocene calcareous nannofossil distribution patterns in the Western Mediterranean. In Kastens,

- K.A., Mascle, J., et al., *Proc. ODP, Sci. Results*, 107: College Station, TX (Ocean Drilling Program), 513–533.
- Roth, P.H., 1973. Calcareous nannofossils—Leg 17, Deep Sea Drilling Project. In Winterer, E.L., Ewing, J.I., et al., *Init. Repts. DSDP*, 17: Washington (U.S. Govt. Printing Office), 695–795.
- Ruckebusch, G., 1983. A Kalman filtering approach to natural gamma ray spectroscopy in well logging. *IEEE Trans. Autom. Control*, AC-28:372–380.
- Schlumberger, 1989. *Log Interpretation Principles/Applications*: Houston, TX (Schlumberger Educ. Services).
- Schweitzer, J.S., Grau, J.A., and Hertzog, R.C., 1988. Precision and accuracy of short-lived activation measurements for in situ geological analyses. *J. Trace Microprobe Techniques*, 6:437–451.
- Scott, H.D., and Smith, M.P., 1973. The aluminum activation log. *Log Analyst*, 14:3–12.
- Serra, O., 1984. *Fundamentals of Well-Log Interpretation* (Vol. 1): *The Acquisition of Logging Data*: Dev. Pet. Sci., 15A: Amsterdam (Elsevier).
- , 1989. *Formation MicroScanner Image Interpretation*: Houston (Schlumberger Educ. Services), SMP-7028.
- Shackleton, N.J., Berger, A., and Peltier, W.A., 1990. An alternative astronomical calibration of the lower Pleistocene timescale based on ODP Site 677. *Trans. R. Soc. Edinburgh: Earth Sci.*, 81:251–261.
- Sissingh, W., 1977. Biostratigraphy of Cretaceous calcareous nannoplankton. *Geol. Mijnbouw*, 56:37–50.
- Spezzaferri, S., 1994. Planktonic foraminiferal biostratigraphy and taxonomy of the Oligocene and lower Miocene in the oceanic record: an overview. *Palaeontographica Ital.*, 81:1–187.
- Spiegler, D., and Rögl, F., 1992. Bolboforma (Protozoa, incertae sedis) In Oligozän und Miozän des Mediterran und der Zentralen Paratethys. *Ann. Naturhist. Mus. Wien*, 94:59–95.
- Sprovieri, R., 1992. Mediterranean Pliocene biochronology: a high resolution record based on quantitative planktonic foraminifera distribution. *Riv. Ital. Paleontol. Stratigr.*, 98:61–100.
- , 1993. Pliocene–early Pleistocene astronomically forced planktonic foraminifera abundance fluctuations and chronology of Mediterranean calcareous plankton bio-events. *Riv. Ital. Paleontol. Stratigr.*, 99:371–414.
- Sprovieri, R., Di Stefano, E., Riggi, A., and Busalacchi, P., in press. La sezione intra-pliocenica di Gibil-Gabel (Caltanissetta, Sicilia Centrale): un esercizio di biostratigrafia ad alta risoluzione. *Boll. Soc. Paleont. Ital.*
- Theodoridis, S., 1984. Calcareous nannofossil biozonation of the Miocene and revision of the helicoliths and discoasters. *Utrecht Micropaleontol. Bull.*, 32:1–271.
- Timur, A., and Toksöz, M.N., 1985. Downhole geophysical logging. *Annu. Rev. Earth Planet. Sci.*, 13:315–344.
- Von Herzen, R.P., and Maxwell, A.E., 1959. The measurement of thermal conductivity of deep-sea sediments by a needle-probe method. *J. Geophys. Res.*, 64:1557–1563.
- Wentworth, C.K., 1922. A scale of grade and class terms of clastic sediments. *J. Geol.*, 30:377–392.

Ms 160IR-103